Proteomic and 3D structure analyses highlight the C/D box snoRNP assembly mechanism and its control

Jonathan Bizarro,[1]* Christophe Charron,[2]* Séverine Boulon,[3] Belinda Westman,[4] Bérengère Pradet-Balade,[1] Franck Vandermoere,[5,6,7] Marie-Eve Chagot,[2] Marie Hallais,[1] Yasmeen Ahmad,[4] Heinrich Leonhardt,[8,9] Angus Lamond,[4] Xavier Manival,[2] Christiane Branlant,[2] Bruno Charpentier,[2] Céline Verheggen,[1] and Edouard Bertrand[1]

[1]Equipe labellisée Ligue contre le Cancer, Centre National de la Recherche Scientifique Unité Mixte de Recherche 5535, Institut de Génétique Moléculaire de Montpellier, 34293 Montpellier, Cedex 5, France
[2]Ingénierie Moléculaire et Physiopathologie Articulaire, Centre National de la Recherche Scientifique Unité Mixte de Recherche 7365, Université de Lorraine, Biopôle de l'Université de Lorraine, 54505 Vandoeuvre-les-Nancy Cedex, France
[3]Centre de Recherches de Biochimie Macromoléculaire, Unité Mixte de Recherche 5237, 34293 Montpellier, Cedex 5, France
[4]Centre for Gene Regulation and Expression, University of Dundee, Dundee DD1 5EH, Scotland, UK
[5]Centre National de la Recherche Scientifique Unité Mixte de Recherche 5203, Institut de Génomique Fonctionnelle, F-34000 Montpellier, France
[6]Institut National de la Santé et de la Recherche Médicale, U661, F-34000 Montpellier, France
[7]Unité Mixte de Recherche 5203, Université de Montpellier 1 and Université de Montpellier 2, F-34000 Montpellier, France
[8]Munich Center for Integrated Protein Science (CiPS[M]) and [9]Department of Biology, Ludwig Maximilians University Munich, 82152 Planegg-Martinsried, Germany

In vitro, assembly of box C/D small nucleolar ribonucleoproteins (snoRNPs) involves the sequential recruitment of core proteins to snoRNAs. In vivo, however, assembly factors are required (NUFIP, BCD1, and the HSP90–R2TP complex), and it is unknown whether a similar sequential scheme applies. In this paper, we describe systematic quantitative stable isotope labeling by amino acids in cell culture proteomic experiments and the crystal structure of the core protein Snu13p/15.5K bound to a fragment of the assembly factor Rsa1p/NUFIP. This revealed several unexpected features: (a) the existence of a protein-only pre-snoRNP complex containing five assembly factors and two core proteins, 15.5K and Nop58; (b) the characterization of ZNHIT3, which is present in the protein-only complex but gets released upon binding to C/D snoRNAs; (c) the dynamics of the R2TP complex, which appears to load/unload RuvBL AAA$^+$ adenosine triphosphatase from pre-snoRNPs; and (d) a potential mechanism for preventing premature activation of snoRNP catalytic activity. These data provide a framework for understanding the assembly of box C/D snoRNPs.

Introduction

Noncoding RNP particles form the molecular machines effecting mRNA splicing and protein synthesis, and they also play regulatory roles at multiple steps during gene expression. Many noncoding RNPs are stable assemblies, and several studies have revealed that their formation requires dedicated cellular machineries, even when the RNP can be assembled in vitro from purified components (Meister et al., 2001). One of the best studied cases is the formation of the heptameric Sm ring on spliceosomal small nuclear RNAs by the SMN (survival of motor neurons) complex (Fischer et al., 1997, 2011). Exhaustive studies on this model system have shown that assembly factors perform multiple roles (Battle et al., 2006; Chari et al., 2008; Yong et al., 2010; Zhang et al., 2011; Grimm et al., 2013). First, they facilitate RNP formation by preassembling core proteins in the absence of RNA, thereby stabilizing labile assembly intermediates. Second, they provide a structural scaffold and organize Sm proteins in a manner that promotes assembly with the target

*J. Bizarro and C. Charron contributed equally to this paper.

Correspondence to Céline Verheggen: celine.verheggen@igmm.cnrs.fr; or Edouard Bertrand: edouard.bertrand@igmm.cnrs.fr

Abbreviations used in this paper: FT, Fourier transform; IP, immunoprecipitation; MS, mass spectrometry; SILAC, stable isotope labeling by amino acids in cell culture; snoRNP, small nucleolar RNP; sRNP, small RNP.

The Rockefeller University Press $30.00
J. Cell Biol. Vol. 207 No. 4 463–480
www.jcb.org/cgi/doi/10.1083/jcb.201404160

RNAs. Third, they prevent nonspecific RNA binding. Hence, by interacting at multiple sites with the core RNP proteins and the target RNAs, RNP assembly factors ensure efficiency, specificity, and quality control of RNP production.

H/ACA small nucleolar RNPs (snoRNPs) are another well-studied class of noncoding RNPs (Kiss et al., 2006, 2010; Terns and Terns, 2006; Liang and Li, 2011; Watkins and Bohnsack, 2012). Studies of their biogenesis also revealed the formation of a protein-only complex containing some core proteins and assembly factors (Wang and Meier, 2004; Li et al., 2011a; Walbott et al., 2011). These studies also showed the involvement of a general assembly machinery, the HSP90–R2TP chaperone complex (King et al., 2001; Boulon et al., 2008), and in particular the role of its AAA^+ ATPases RuvBL1 and RuvBL2, which promote dissociation of the assembly factor SHQ1 (Machado-Pinilla et al., 2012). Finally, it was found that the pre-snoRNP factor NAF1 inhibits the activity of the immature RNP particle (Grozdanov et al., 2009; Walbott et al., 2011).

In contrast to the cases of snRNPs and H/ACA snoRNPs in which protein-only complexes are preformed by assembly factors, in vitro studies of box C/D snoRNPs have suggested an ordered assembly pathway that takes place directly on the snoRNA (Schultz et al., 2006). Box C/D snoRNPs catalyze 2′-*O*-methylation of target RNAs (Cavaillé et al., 1996; Kiss-László et al., 1996; Kiss et al., 2006; Terns and Terns, 2006; Liang and Li, 2011; Watkins and Bohnsack, 2012). They contain four core proteins assembled around a pseudodimeric guide snoRNA, which contains a C/D and a C′/D′ motif. In humans, box C/D snoRNPs are composed of the protein 15.5K, which directly recognizes the snoRNA K-turn (kink turn) C/D motif (Watkins et al., 2000), and Nop56/Nop58, two homologous proteins that each bind a copy of the 2′-*O*-methylase Fibrillarin (Aittaleb et al., 2003). Nop56 and Nop58 contain a coiled-coil domain, which allows them to heterodimerize, thereby connecting the C/D and C′/D′ RNA motifs and creating the pseudodimeric structure of the snoRNP (Aittaleb et al., 2003; Lin et al., 2011). Nop56 and Nop58 also contain a Nop domain, which is an RNP binding module that interacts with a preformed 15.5K–snoRNA complex (Liu et al., 2007). Several in vitro studies have led to the hypothesis that snoRNP assembly is initiated by the binding of the 15.5K to the snoRNA C/D motif followed by recruitment of the Nop58/Fibrillarin dimer, interaction with Nop56/Fibrillarin bound at the C′/D′ motif, and formation of the mature, active structure (Watkins et al., 2002). In vivo, assembly of C/D snoRNP requires several assembly factors: the HSP90–R2TP chaperone complex that is also required for H/ACA snoRNP biogenesis (Newman et al., 2000; Boulon et al., 2008; Zhao et al., 2008) and two specific factors, NUFIP, which connects the 15.5K to the R2TP (Boulon et al., 2008; Rothé et al., 2014), and BCD1, whose function remains poorly characterized (Peng et al., 2003). Nop58 and/or 15.5K are probable clients of HSP90 (Boulon et al., 2008), and the RuvBL1/RuvBL2 subunits of the R2TP complex have been hypothesized to catalyze a remodeling event on the immature C/D snoRNP (Watkins et al., 2004; Boulon et al., 2008). In agreement, they make ATP-dependent interactions with core C/D proteins and other assembly factors (McKeegan et al., 2009; Cheung et al., 2010). However, the nature of this remodeling event and more generally how the assembly factors function and what is the in vivo assembly pathway of box C/D snoRNPs have remained poorly characterized. Here, we use quantitative proteomics and structural biology to identify key features of snoRNP biogenesis: an early protein-only complex that contains 15.5K and Nop58 together with assembly factors and a late step leading to the release of NUFIP and the activation of snoRNP catalytic activity.

Results

hBCD1 SILAC proteomics identifies ZNHIT3 as a new C/D snoRNP assembly factor

To characterize the C/D snoRNP assembly pathway in vivo, we performed stable isotope labeling by amino acids in cell culture (SILAC) proteomic experiments using a variety of snoRNP assembly factors as baits. We initiated our analysis with Bcd1p, an essential protein in yeast that is required for the accumulation of box C/D snoRNPs (Peng et al., 2003), but whose function is poorly characterized. We cloned the human homologue of BCD1 (ZNHIT6, referred to as hBCD1; see Table S1 for the nomenclature), fused it to GFP, and stably expressed it in U2OS cells. Cell extracts were fractionated using differential detergent treatments, to yield a first fraction extracted in 0.1% NP-40 that contains cytoplasmic and highly soluble nucleoplasmic material (referred to as "more extractable fraction"), and a second fraction, sonicated and extracted in 1% NP-40 and 0.5% deoxycholate and which contains less easily extractable nucleoplasmic material together with nucleoli (Boulon et al., 2010b; "less extractable fraction"). Each fraction was immunoprecipitated using anti-GFP antibodies and analyzed by quantitative mass spectrometry (MS) against a control purification performed simultaneously with the parental U2OS cells (Fig. 1 A). Proteins were considered as hits if they had a SILAC ratio (specific immunoprecipitation [IP]/control IP) >3.5 or if their SILAC ratio was between 1.5 and 3.5 but with a frequency of detection in unrelated IPs of <25% (see Boulon et al., 2010a; hit lists in Table S3). In the highly extractable fraction, five proteins stood out from the background: the bait GFP-hBCD1, the R2TP components RuvBL1 and RuvBL2, the snoRNP assembly factor NUFIP, and a small HIT Zn-finger protein not previously implicated in snoRNP biogenesis: ZNHIT3. In the less extractable fraction, less bait was recovered, and only RuvBL1 could be identified as a specific partner. The protein 15.5K was also detected in the IP, albeit with low SILAC ratio, and the specificity of this interaction was thus verified by IP/Western blotting (Fig. S1 A). To investigate the protein–protein interactions responsible for the formation of these complexes, we performed yeast two-hybrid assays (Fig. 1 B). This revealed a specific interaction between hBCD1 and RuvBL2, which was consistent with the large amount of RuvBL proteins copurifying with hBCD1 in the SILAC assay and with previous protein–protein interaction data (McKeegan et al., 2007). We also observed an interaction between NUFIP and ZNHIT3 (Fig. 1 B). This interaction did not involve the PEP domain of NUFIP that binds 15.5K, and this suggested that a ternary complex could be formed between NUFIP, ZNHIT3, and 15.5K. In agreement,

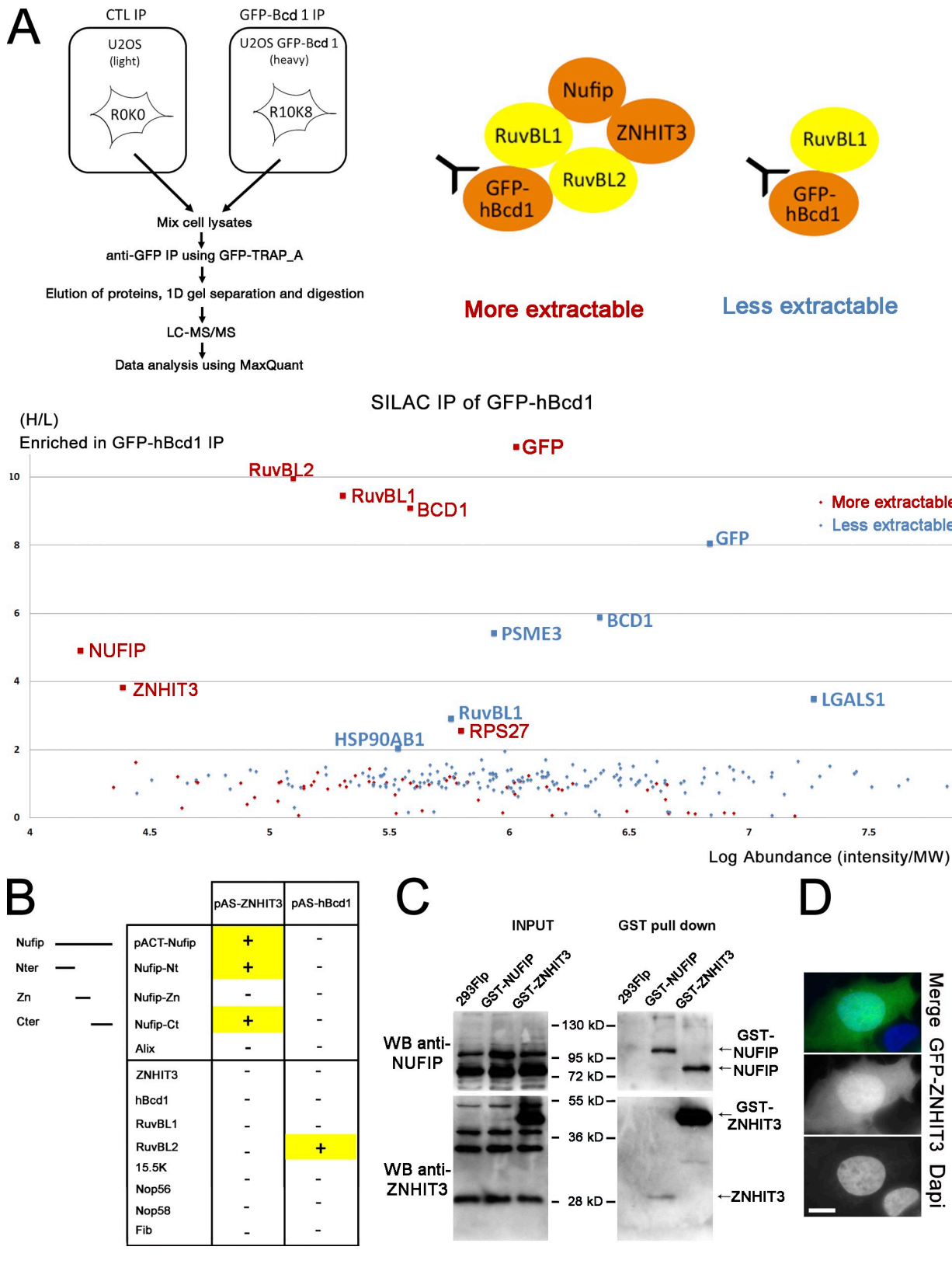

Figure 1. **hBCD1 identifies a new snoRNP assembly factor.** (A) GFP-hBCD1 was purified from more and less extractable fractions of U2OS cells, and pellets were analyzed by SILAC proteomic. X axis: protein abundance (Log_{10}); Y axis: SILAC ratios (specific vs. control IP). LC, liquid chromatography; H/L, heavy/light; MW, molecular weight. (B) Yeast two-hybrid assays with ZNHIT3, hBCD1, and snoRNP assembly factors and core proteins. Alix is used as a negative control. Fib, Fibrillarin; Nter, N terminal; Cter, C terminal. (C) Co-IP assays between NUFIP and ZNHIT3. Extracts from 293T cells stably expressing GST-NUFIP and GST-ZNHIT3 were purified on glutathione beads and analyzed by Western blots (WB). (D) Intracellular localization of GFP-ZNHIT3. Microscopy images of HeLa cells transfected with a GFP-ZNHIT3 expression vector and labeled with DAPI to stain nuclei. Bar, 10 μm.

when NUFIP was coexpressed in the two-hybrid strain, an interaction could be detected between 15.5K and ZNHIT3 (Fig. S1 B). The interaction between NUFIP and ZNHIT3 appeared conserved throughout evolution because the yeast homologues of these proteins, Rsa1p and Hit1p, were also reported to interact in high-throughput interaction datasets (Ito et al., 2001), and we could confirm that this is a direct interaction by GST pull-down with proteins produced in vitro (Fig. S1 C). To further confirm the interaction between NUFIP and ZNHIT3, we coprecipitated the two proteins (Fig. 1 C). Extracts from stable clones of 293T cells expressing GST-tagged versions of either NUFIP or ZNHIT3 were immunopurified using glutathione beads and analyzed by Western blots with NUFIP and ZNHIT3 antibodies. NUFIP copurified with GST-ZNHIT3, and conversely, ZNHIT3 copurified with GST-NUFIP. We then determined the intracellular localization of GFP-ZNHIT3 in transiently transfected cells using fluorescence microscopy. ZNHIT3 localized mainly in the nucleoplasm with some cytoplasmic staining, in a manner similar to the localization of NUFIP (Bardoni et al., 1999). Collectively, these data indicate that ZNHIT3 is a partner of NUFIP, and its copurification with hBCD1 suggested a role in C/D snoRNP biogenesis.

ZNHIT3 proteomics identifies an RNase-resistant complex composed of two C/D core proteins and five assembly factors

To explore the role of ZNHIT3, we performed a proteomic experiment using GFP-ZNHIT3 as the bait. In this experiment, we used a triple SILAC encoding scheme to compare RNase-treated and untreated extracts and to determine the contribution of RNA in the complexes observed (Figs. 2 A and S2, A and B). We first focused on the untreated extracts. In the less extractable fraction, little of the bait was recovered, and only NUFIP and some proteasomal subunits could be identified with high specificity and high SILAC ratios. In the more extractable fraction, however, the six proteins previously identified with hBCD1 as the bait were also found (NUFIP, RuvBL1, RuvBL2, hBCD1, ZNHIT3, and 15.5K), and we additionally detected the C/D core protein Nop58. This indicated that the hBCD1 and ZNHIT3 complexes represent a similar entity, which would thus be composed of five assembly factors bound to two core proteins.

To investigate the presence of nascent snoRNA in the GFP–ZNHIT3 complex, we compared immunopurifications performed with and without RNase treatment. When the SILAC ratios measuring the enrichment over control were plotted against one another, all seven proteins of the complex were found on the diagonal of the plot, indicating that their association with ZNHIT3 was not affected by the RNase treatment (Fig. 2 B; similar results were obtained using protein abundance instead of SILAC ratio, Fig. S2 A). This was further confirmed by transfecting GFP-15.5K, GFP-Nop58, and GFP-hBCD1 in 293T cells and by analyzing the coprecipitated proteins by Western blot, either with, or without, RNase treatment. Indeed, all three proteins coprecipitated NUFIP, ZNHIT3, and RuvBL1, and their association was not affected by the presence or absence of RNase (Fig. 2 C). Thus, these results raised the possibility that the ZNHIT3 complex was a protein-only molecular assembly. In the following, we refer to pre-snoRNPs complexes as a general term whether these complexes contain snoRNAs or not.

ZNHIT3 associates preferentially with assembly-defective U3 snoRNAs

To investigate more directly the association of ZNHIT3 with C/D snoRNAs, we measured its binding to U3 by RNase protection assays and compared it to other assembly factors. A rat U3 gene was transfected in HeLa cells, either alone, or with tagged versions of ZNHIT3, RuvBL1, or hBCD1. Extracts were immunoprecipitated using appropriate antibodies, and the pelleted RNAs were analyzed with a probe covering the 3′ end of rat U3, such that both precursor and mature forms of the snoRNA could be identified and discriminated from the endogenous human U3 (Boulon et al., 2004). We used two forms of U3: a wild-type gene and mutant carrying three point mutations in stem II (U3mut6; Fig. 3 A), which were previously shown to reduce association with Nop56, Nop58, and Fibrillarin (Watkins et al., 2002). In agreement, it prevented most of the accumulation of U3 snoRNA in the nucleolus (Fig. 3 B), and it led to the accumulation of the precursor forms of U3 at the expense of the mature form (Fig. 3, C–F, compare U3-I, U3-II, and U3-m in the input lanes). This mutant was thus mostly defective for assembly, although not completely inactive. We found that NUFIP, hBCD1, and RuvBL1 bound similarly to precursors and mature forms of rat U3 (Fig. 3, C–F). In contrast, we failed to detect an association of ZNHIT3 with either the precursor, or mature forms, of wild-type U3 (Fig. 3 D). Unexpectedly, however, we could observe binding of ZNHIT3 to the precursor forms of the U3mut6 mutant. Collectively, these data suggest that the protein complex identified with ZNHIT3 is indeed devoid of snoRNAs and that binding of this complex to wild-type U3 induces the loss of ZNHIT3. In the case of U3mut6, assembly of the complete snoRNP is delayed, and ZNHIT3 remains in the complex. This indicates an assembly scheme in which a protein-only complex composed of ZNHIT3, hBCD1, NUFIP, RuvBL1/2, Nop58, and 15.5K binds nascent snoRNAs and then rapidly releases ZNHIT3, whereas NUFIP and RuvBL1/2 remain bound until late stages of maturation. Hence, the protein-only pre-snoRNP complex appears to be remodeled upon its binding to nascent snoRNAs.

GFP-NUFIP proteomics reveals association with splicing factors

To further characterize the assembly pathway of box C/D snoRNPs, we performed a SILAC experiment using GFP-NUFIP as the bait (Fig. 4 A). In the highly extractable fraction, we detected large amounts of ZNHIT3 and a weaker association with the snoRNP core proteins 15.5K and Nop58. Given the strong association of ZNHIT3 with both the RuvBL1/2 proteins and NUFIP, the absence of RuvBL1/2 in the NUFIP SILAC was surprising. This could be caused either by a lack of association with NUFIP, by a dissociation of these proteins during cell fractionation, or by a limited sensitivity of our proteomic experiment. To test these possibilities, we immunopurified GFP-NUFIP in various conditions and analyzed for the presence of RuvBL1 and RuvBL2 by Western blotting. Both proteins copurified with GFP-NUFIP,

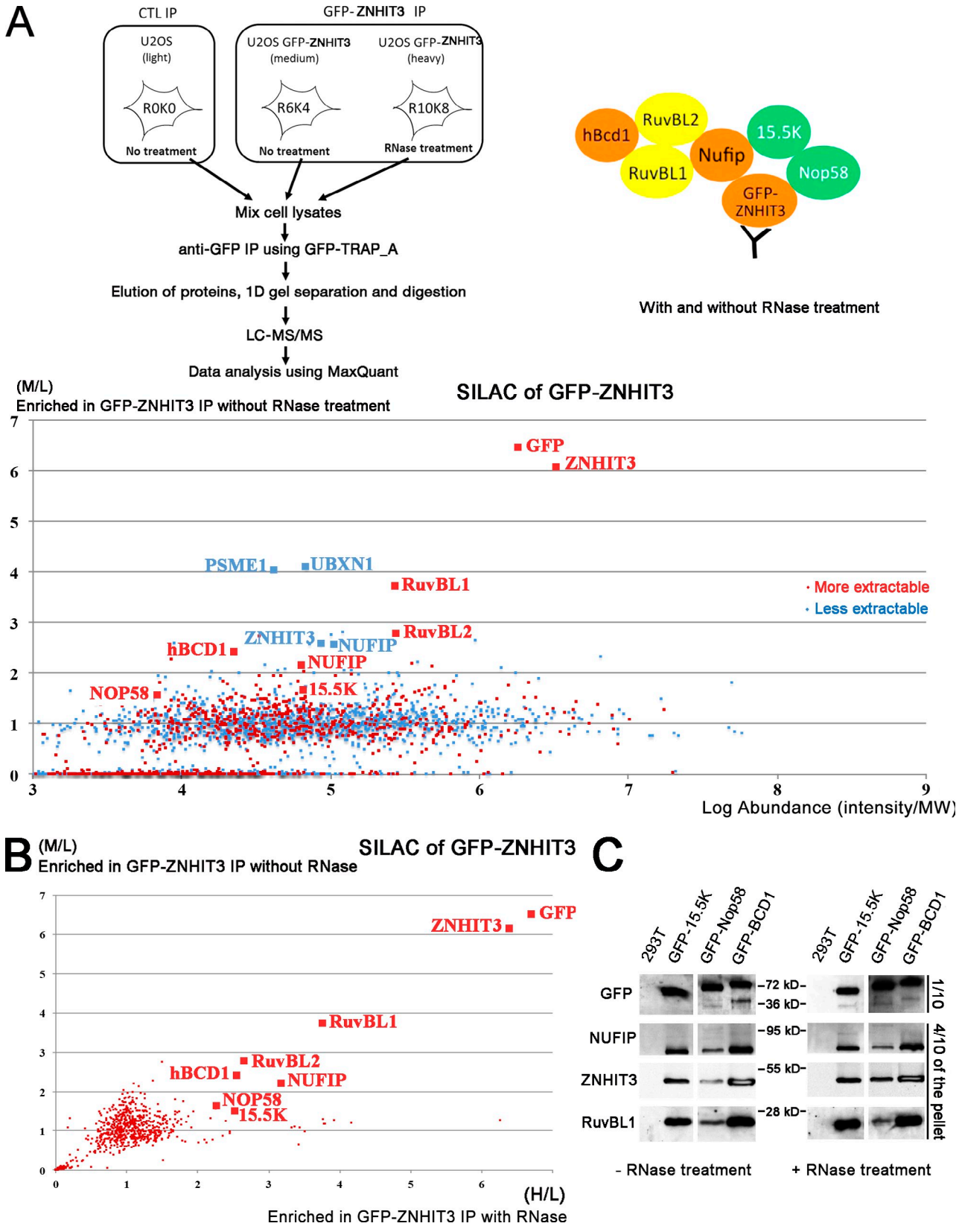

Figure 2. **ZNHIT3 forms a complex containing Nop58 and 15.5K as well as five assembly factors.** (A) Proteomic analysis of GFP-ZNHIT3. X axis: protein abundance (Log_{10}); Y axis: SILAC ratios (specific vs. control IP). LC, liquid chromatography; M/L, medium/light; MW, molecular weight. (B) Proteomic analysis of GFP-ZNHIT3, in the presence and absence of RNase treatment. X axis: SILAC ratios (specific vs. control IP) in the presence of RNase treatment; Y axis: SILAC ratios (specific vs. control IP) in the absence of RNase treatment. H/L, heavy/light. (C) Co-IP assays with GFP-NUFIP, GFP-hBCD1, and GFP-15.5K. 293T cells were transiently transfected with the indicated proteins, extracts were purified on GFP-TRAP beads, and pellets were analyzed by Western blots with the indicated antibodies. When indicated, extracts were treated with 0.6 µg/ml RNase. Pellets: 5% of inputs.

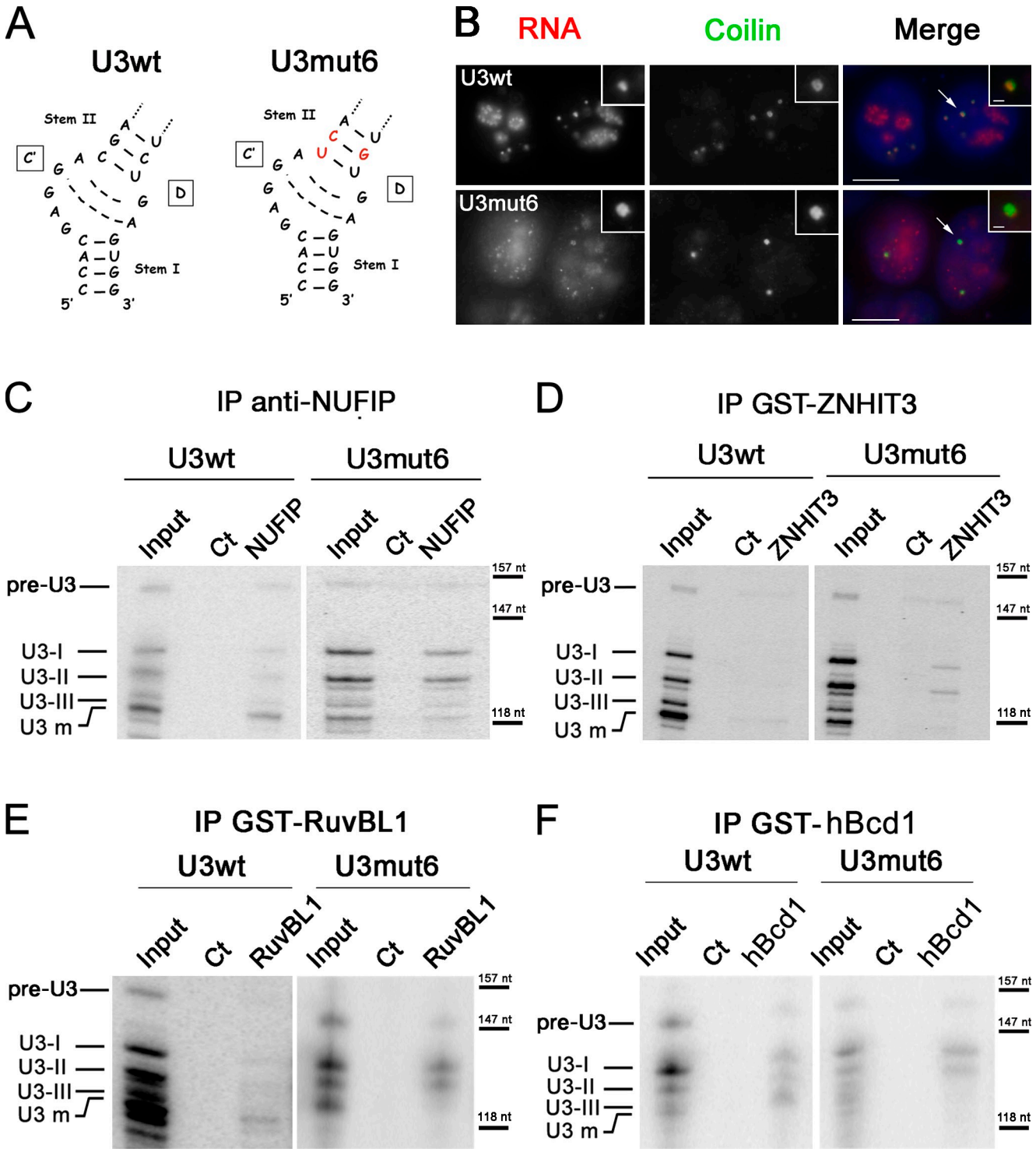

Figure 3. **ZNHIT3 associates preferentially with assembly defective U3 snoRNAs.** (A) Schematic of the U3mut6 mutant. (B) Intracellular localization of U3mut6. HeLa cells were transfected with the U3wt and U3mut6 gene and hybridized in situ with a probe specific for the transfected rat U3 gene. Arrows on the merged image point to a Cajal body that is zoomed in the insets. Bars: (main images) 10 µm; (insets) 0.6 µm. (C–F) Binding of NUFIP (C), ZNHIT3 (D), RuvBL1 (E), and hBCD1 (F) to U3 snoRNAs. HeLa cells were transfected with the indicated plasmids, extracts were immunopurified on glutathione beads, and RNAs in the pellet were analyzed by RNase protection with a probe covering the 3′ end of the transfected rat U3 gene. Ct: control IP with empty beads. Pre-U3-I, pre-U3-II, and pre-U3-III: precursor forms of U3 snoRNA. U3m: mature form of U3. Pellets: 5% of inputs.

but they could be detected only when the extracts were not fractionated (Fig. 4 B). This suggested that the association of RuvBL1/2 with NUFIP was more labile than those formed with ZNHIT3 or hBCD1.

Interestingly, several differences were observed between the more and the less extractable fraction of GFP-NUFIP immunopurifications (Fig. 4 A). First, additional proteins were detected in the less extractable fraction: Fibrillarin, the core

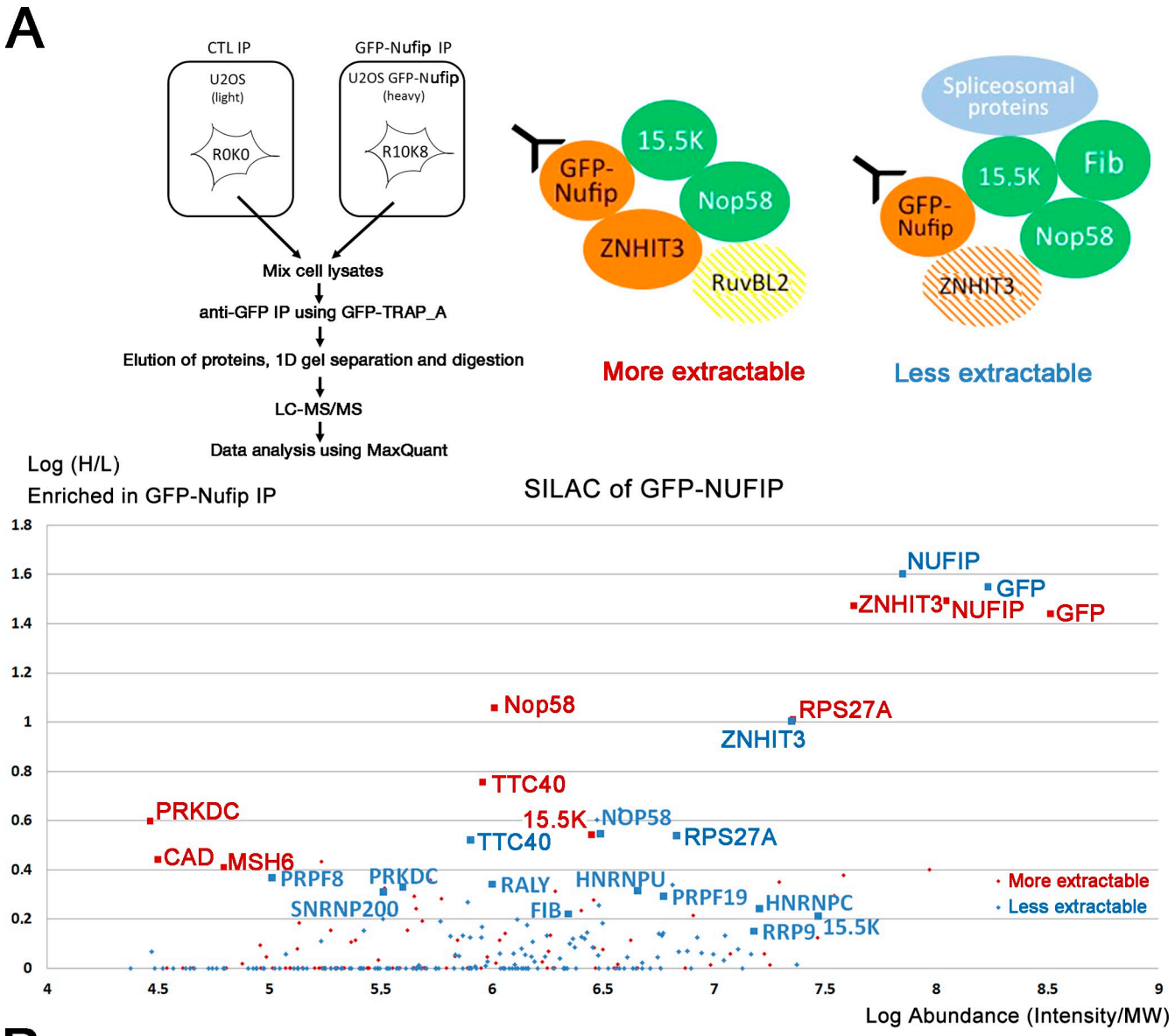

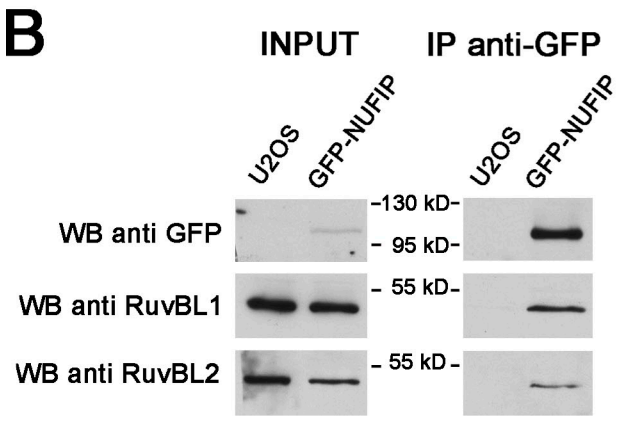

Figure 4. **SILAC proteomic analysis of GFP-NUFIP reveals binding to snoRNAs.** (A) Proteomic analysis of GFP-NUFIP. X axis: protein abundance (Log_{10}); Y axis: SILAC ratios (Log_{10} specific vs. control IP). CTL, control; LC, liquid chromatography; H/L, heavy/light; MW, molecular weight. (B) Co-IP assays with GFP-NUFIP. U2OS cells were extracted in HNTG, extracts were purified on GFP-TRAP beads, and pellets were analyzed by Western blots (WB) with the indicated antibodies. Pellets: 5% of inputs.

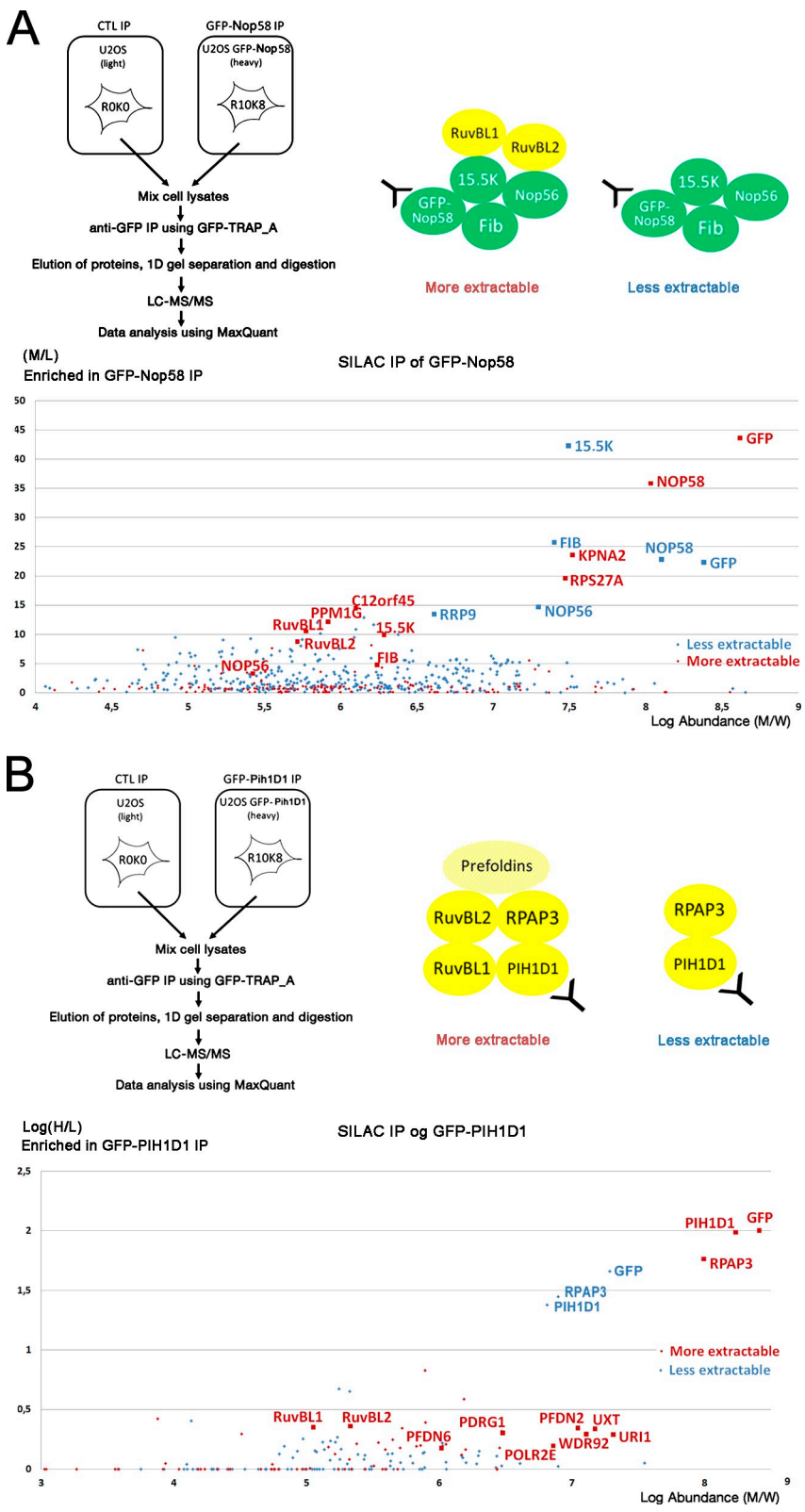

Figure 5. **SILAC proteomic analyses of GFP-Nop58 and GFP-PIH1D1.** (A) Proteomic analysis of GFP-Nop58. X axis: protein abundance (Log_{10}); Y axis: SILAC ratios (specific vs. control IP). (B) Proteomic analysis of GFP-PIH1D1. X axis: protein abundance (Log_{10}); Y axis: SILAC ratios (Log_{10} specific vs. control IP). Legend as in A. CTL, control; LC, liquid chromatography; H/L, heavy/light; M/L, medium/light; Fib, Fibrillarin; MW, molecular weight.

snoRNP protein that binds Nop58, and a set of splicing factors, including PRPF8, PRPF19, SNRPD1, and SNRNP200. Because most C/D snoRNPs are produced from introns in humans (Matera et al., 2007), this suggested that in this fraction, GFP-NUFIP is associated with snoRNAs. This was also consistent with the detection of RRP9 (also called U3-55K). This protein binds to the B/C motif of U3 (Lukowiak et al., 2000), a very abundant non-intronic C/D snoRNA. Second, the amount of ZNHIT3 copurifying with GFP-NUFIP decreased by more than twofold in the less extractable fraction, whereas at the same time the amount of Nop58 and 15.5K increased by three- and eightfold, respectively (Fig. 4). This was in agreement with the

aforementioned data, which indicated a loss of ZNHIT3 upon binding of the protein-only complex to snoRNAs. The results obtained with GFP-NUFIP thus suggested a progression in snoRNP assembly, in which the protein-only complex becomes bound to nascent snoRNA, leading to ZNHIT3 dissociation and reinforcement of Fibrillarin association.

The release of RuvBL1/2 is a late step during assembly of C/D snoRNPs

To complete our analysis of the assembly pathway of box C/D snoRNPs, we performed a SILAC proteomic analysis of GFP-Nop58 (Fig. 5 A). In the less extractable fraction, which is expected to contain nucleoli-derived complexes, we detected the three other C/D core proteins, 15.5K, Fibrillarin, and Nop56, all with high SILAC ratios and high abundance (similar that of the bait itself). We also detected many proteins known to associate with U3, such as RRP9 (U3-55K), La/SSB, and the SSU processosome, indicating that the complexes purified consisted of mature C/D snoRNPs. Consistently, we also detected many nucleolar proteins. In the more extractable fraction, which contains cytoplasmic and nucleoplasmic material, we also detected a specific enrichment of all snoRNP core proteins, including Nop56. They were, however, present in ∼10–100-fold lower abundance relative to Nop58 when compared with the less extractable fraction. We also detected RRP9 and La/SSB, which indicated the presence of U3 snoRNA. We also found RuvBL1/RuvBL2, in amounts larger than Nop56. A novel protein, c12orf45, was also present in high abundance and with a high SILAC ratio. This protein is conserved throughout evolution down to *Schizosaccharomyces pombe* (NCBI EST gene ID 14217966), and it was also previously copurified with RuvBL1 and RuvBL2 (Jeronimo et al., 2007). By performing systematic pairwise two-hybrid tests, we found that it makes a specific interaction with RuvBL1 (Fig. S2 C), and it thus represents a potential new snoRNP assembly factor. The presence of all four core proteins in this complex, together with snoRNAs and RuvBL1/RuvBL2, indicates that this is a late assembly intermediate.

To confirm that c12orf45 is a snoRNP assembly factor, we performed a time-resolved proteomic experiment using a triple SILAC encoding scheme. We transiently transfected HeLa cells with a GFP-Nop58 construct for 10 h, pulled down the associated proteins, and compared them with the proteins bound to a version of GFP-Nop58 that was stably expressed in cells. A plot of the SILAC ratios at 10 h versus the ones at steady-state shows that RuvBL1/2 and c12orf45 preferentially associate with GFP-Nop58 at 10 h, whereas nucleolar proteins associate more strongly at steady state (Fig. S2 D). This indicates that RuvBL1/2 and c12orf45 associate transiently with nascent Nop58 protein.

Proteomic analysis of PIH1D1 identifies the R2TP–prefoldin-like complex

The R2TP complex has been previously involved in snoRNP biogenesis (Zhao et al., 2005, 2008; Boulon et al., 2008). In humans, it is composed of the conserved core R2TP complex (RuvBL1/RuvBL2, PIH1D1, and RPAP3), together with a set of prefoldins and few other proteins (Boulon et al., 2008, 2010b; Cloutier et al., 2009). Our proteomic analyses readily detected the RuvBL1/RuvBL2 proteins in most of the pre-snoRNP complexes identified in this paper (i.e., both the protein-only and the RNA-bound complexes) but failed to detect other components of the R2TP complex, despite their known role in snoRNP biogenesis and interactions with C/D core proteins (Gonzales et al., 2005; Boulon et al., 2008; Zhao et al., 2008; McKeegan et al., 2009). One reason could be that the interaction between the RuvBL proteins and PIH1D1/RPAP3 is too labile to survive our purification conditions. To test this possibility, we performed a SILAC experiment using GFP-PIH1D1 as the bait (Fig. 5 B). In the more extractable fraction, we found large amounts of RPAP3 and nearly all components of the R2TP–prefoldin-like complex, including the key RuvBL1/RuvBL2 proteins. This indicated that the failure to detect PIH1D1 and RPAP3 in the other purifications was not caused by poor stability of the R2TP complex. The purification of PIH1D1 from the less extractable fraction yielded about tenfold less bait, and it was thus difficult to assess reliably the presence or absence of putative partners. We, however, noted that large amounts of RPAP3 still copurified with PIH1D1, suggesting that these two proteins form a stable heterodimer in cells, as they do in vitro (Zhao et al., 2005; Boulon et al., 2008; Eckert et al., 2010).

Meta-analysis of the SILAC proteomic data

Next, we pooled together our proteomic data and performed a meta-analysis to identify protein subcomplexes. First, a graph was made to recapitulate the main interactions found in the proteomic experiments (Fig. 6 A). This nicely showed that NUFIP, ZNHIT3, hBCD1, and RuvBL1/RuvBL2 lie at the heart of the snoRNP assembly mechanism, together with the core proteins 15.5K and Nop58. The R2TP protein lies at the periphery of the network, together with spliceosomal proteins, the other C/D core proteins, and U3-specific proteins. Next, we used the SILAC enrichment data to perform a clustering analysis (Fig. 6 B). Three groups of assembly factors were found. The first corresponds to the NUFIP/ZNHIT3 pair, the second to PIH1D1/RPAP3, and the third to hBCD1/RuvBL1/RuvBL2, with RuvBL1/RuvBL2 placed close to each other. This nicely corresponded to the protein–protein interactions identified from yeast two-hybrid assays or from in vitro reconstitution of protein complexes. Indeed, PIH1D1 interacts with RPAP3 in yeast two-hybrid assays and GST pull-down experiments (Boulon et al., 2008, 2010b), and the yeast proteins form a stable complex in vitro (Zhao et al., 2005; Eckert et al., 2010), whose structure was recently solved (Back et al., 2013; Pal et al., 2014). Likewise, RuvBL1/RuvBL2 are well known to heteromultimerize (Gorynia et al., 2011), and RuvBL2 also directly interacts with hBCD1 in yeast two-hybrid and in vitro assays (this study and McKeegan et al., 2009). Finally, we show here that NUFIP and ZNHIT3 make an evolutionarily conserved interaction. Collectively, this suggests that these modules correspond to protein subcomplexes that form the building blocks of the snoRNP assembly machinery. It is also interesting to note that Nop58 clusters away from the other core C/D snoRNP proteins. This is in line with the idea that it plays a particular role during snoRNP assembly.

Crystal structure of the Snu13p–Rsa1$_{239–265}$ complex

The aforementioned data suggested that several remodeling steps occur during C/D snoRNP biogenesis, and they reinforced

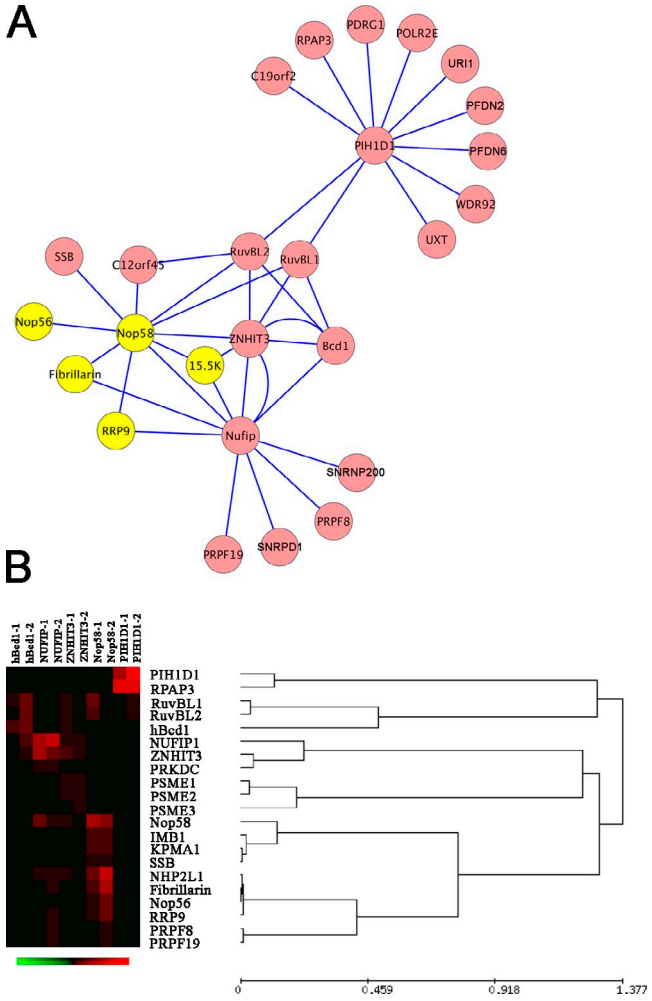

Figure 6. **Meta-analysis of the proteomic data.** (A) Network analysis of the factors involved in snoRNP biogenesis. The interactions detected by SILAC proteomics were used to create an interaction network using Cytoscape. (B) Clustering analysis of the proteomic data. SILAC ratio was used to perform a clustering analysis. Columns: baits, −1 is the less extractable fraction and −2 is the more extractable fraction. Rows: preys.

the idea of a central role of NUFIP. Indeed, NUFIP binds directly to 15.5K (Boulon et al., 2008), the protein that nucleates C/D snoRNP, and it is present through most of the snoRNP assembly pathway, from early protein-only complexes until late assembly intermediates. To better understand the function of NUFIP during snoRNP assembly, we turned to structural approaches. We previously showed that the PEP domain of NUFIP is sufficient to bind to 15.5K and that this interaction is conserved between the yeast proteins (Rsa1p and Snu13p, respectively; Rothé et al., 2014). We found that a fragment of yeast PEP (residues 238–290 of Rsa1p) formed a stable complex with full-length Snu13p and gave high quality crystals after purification to homogeneity (see Materials and methods). The structure was solved by single anomalous diffraction and was refined to a final resolution of 1.55 Å (Table S2).

In the crystal structure, the PEP domain of Rsa1p consists of a long α helix of 17 residues at the N terminus, a short loop of three residues and a short α helix of five residues at the C terminus. The N-terminal α helix of $Rsa1_{239–265}$ lies in a groove at the surface of Snu13p that is delineated by the helix α3 and the C-terminal helix α5 (Fig. 7, A and B). Comparison of Snu13p complexed to Rsa1p with Snu13p in a free state (Oruganti et al., 2005; Protein Data Bank [PDB] accession no. 1ZWZ) yields a root-mean-square deviation of Cα positions of 1.28 Å. This is reduced to 0.54 Å without the last 20 residues of Snu13p, indicating a rigid-body movement of ∼3 Å of the C-terminal helix α5 of Snu13p upon binding of $Rsa1_{239–265}$ (Fig. 7 C).

Complementary electrostatic surface potentials favor Snu13p–Rsa1p interaction

The peculiar location of acidic and basic residues of Snu13p results in an asymmetric electrostatic surface potential (Fig. 7 D), with one negatively charged and one positively charged face (the one that binds the K-turn RNA motif). As found for the archaeal homologous L7Ae protein (Charron et al., 2004a,b), this electrostatic property favors RNA–protein association. The electrostatic potential at the surface of $Rsa1_{239–265}$ is almost fully positive (Fig. 7, D–G), and it binds the negatively charged face of Snu13p, which should favor the Snu13p–Rsa1p interaction.

Functionally important hydrophobic and polar interactions at the Snu13p–Rsa1p interface

In the established structure, a single and continuous surface of Snu13p is buried by $Rsa1p_{239–263}$ (Fig. S3). It involves residues of helix α3, strand β3, loop α3-β3, the N-terminal loop, and the C-terminal helix α5. These proteins form four distinct networks of interactions, which are nicely supported by our previous biochemical work. First, residues K118, D119, and E122 in helix α5 of Snu13p form hydrogen bonds with residues S258, N259, and I257 of Rsa1p (Fig. 8 A). Accordingly, I257A substitution in Rsa1p strongly reduces the interaction strength (Rothé et al., 2014). Second, residues L65 and L69 establish hydrophobic contacts with helix α3 in Snu13p and W245 of Rsa1p (Fig. 8 B), explaining why Snu13p L69A and Rsa1p W245A substitution have strong deleterious effects on the interaction (Rothé et al., 2014). Third, in agreement with the need for Snu13p E72 and Rsa1p R249 to form the complex (Rothé et al., 2014), a strong ionic interaction is formed between these residues (Fig. 8 B). Finally, the hydrophobic residue W253 of $Rsa1_{239–265}$ tightly binds in a hydrophobic pocket of Snu13p (Fig. 8 C), which is formed by residues P10, P77, Y78, and K118, I121, E122, and L125 (Fig. 8 D). Interestingly, these last residues are in the helix α5 of Snu13p that moves upon Rsa1p binding, suggesting an important role of this movement.

Interestingly, most of the detected contacts also appear to be conserved in the human proteins (Fig. S4, A and B; Vidovic et al., 2000; Rothé et al., 2014). In particular, W253 in Rsa1p is substituted into a homologous aromatic residue Y247 in NUFIP (Fig. S4), and the structure of 15.5K also reveals a structurally conserved hydrophobic pocket at its surface, with strictly conserved key residues (Vidovic et al., 2000). Finally, the in vivo functional importance of several of the identified interactions is supported by the fact that E72A substitution in Snu13p and R245A and R249A substitution in Rsa1p generate a marked growth defect in yeast and that the Rsa1p W245A substitution

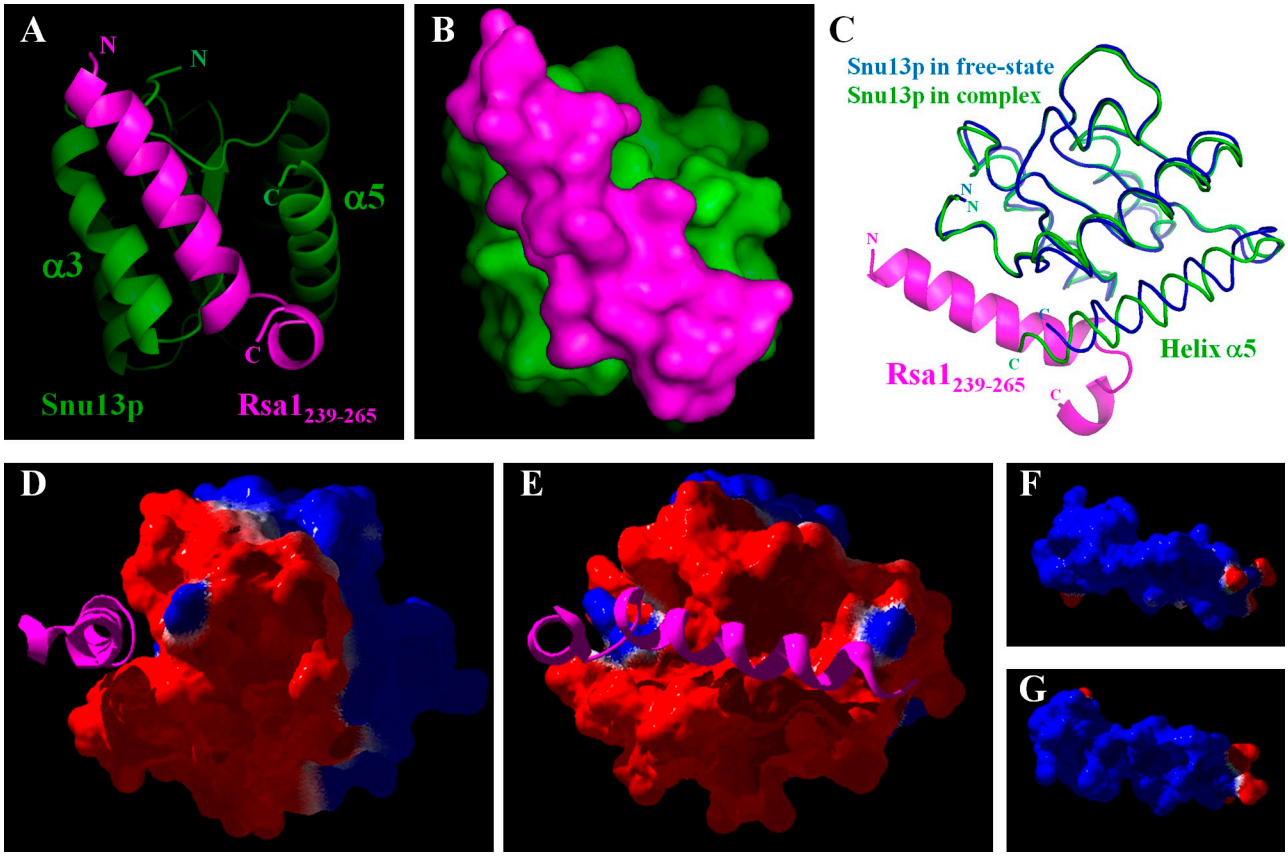

Figure 7. **The PEP domain of Rsa1p lies in a groove at the surface of Snu13p.** (A and B) Ribbon representation (A) and molecular surface (B) of the complex between Snu13p and Rsa1$_{239–265}$, obtained from the crystal structure of the complex. A and B are in the same orientation. (C) Superimposition of Snu13p bound to Rsa1p with Snu13p in free state (PDB no. ZWZ). Upon interaction with Rsa1$_{239–265}$, a rigid-body movement of ∼3 Å of the α5 helix is observed in Snu13p. (D–G) Electrostatic properties of protein Snu13p (D and E) and Rsa1$_{239–265}$ (F and G). The electrostatic potentials were computed by using the algorithm of Boltzmann available on the Swiss-PdbViewer. Blue, white, and red regions correspond to positive, neutral, and negative electrostatic potentials, respectively. (D and E) Electrostatic potential mapped on the molecular surface of Snu13p and viewed in two different orientations (rotation by 90°). Rsa1$_{239–265}$ is shown in magenta in a ribbon representation. (F and G) Electrostatic potential mapped on the molecular surface of Rsa1$_{239–265}$ and viewed in two opposite directions.

strongly reduces the efficiency of box C/D snoRNP biogenesis in yeast (Rothé et al., 2014). Therefore, although established with an Rsa1p fragment, the present 3D structure is strongly supported by previous biochemical and genetic data obtained with full-length proteins.

Rsa1p/NUFIP is predicted to prevent rotation of the catalytic module of box C/D snoRNPs

Up to now, no 3D structure of a complete eukaryotic C/D snoRNP is available. However, several crystal structures of their archaeal counterparts have been recently determined (Ye et al., 2009; Xue et al., 2010; Lin et al., 2011). These particles contain of Fibrillarin, L7Ae (the homologue of Snu13p/15.5K), and NOP5 (the homologue of Nop56 and Nop58). The small RNP (sRNP) particle was found in both catalytically active and inactive states, and both types of structures have been solved at high resolution (Ye et al., 2009; Xue et al., 2010; Lin et al., 2011; Lapinaite et al., 2013). The main difference between these two states involves the catalytic module comprising Fibrillarin and the N-terminal domain of NOP5. Indeed, this module is located far away from the RNA modification site in the inactive state, and it needs to make a large rotation to adopt a catalytically active form (Lin et al., 2011). On the basis of this archaeal structure, a similar architecture can be proposed for human snoRNPs (Fig. 9). Importantly, modeling of the eukaryotic pre-snoRNP complex predicts that the presence of NUFIP should be compatible with the structure of C/D snoRNPs in an open inactive form (Fig. 9, left). However, according to these structural predictions, the rotation of the catalytic module that is required to adopt a closed active form of the C/D snoRNP would lead to a steric clash between the second α helix of the PEP domain of NUFIP and the N-terminal domain of Nop58 (Fig. 9, right). Thus, the presence of NUFIP (or Rsa1p in yeast) in the pre-snoRNP complexes is expected to prevent formation of the catalytically active structure and to inhibit their catalytic activity. A formal demonstration that this is the case will, however, require additional studies with eukaryotic C/D snoRNPs: the resolution of their structure or the development of a suitable in vitro methylation assay.

Discussion

How box C/D snoRNPs are assembled in vivo is not well understood. Here, by using a combination of SILAC proteomics and

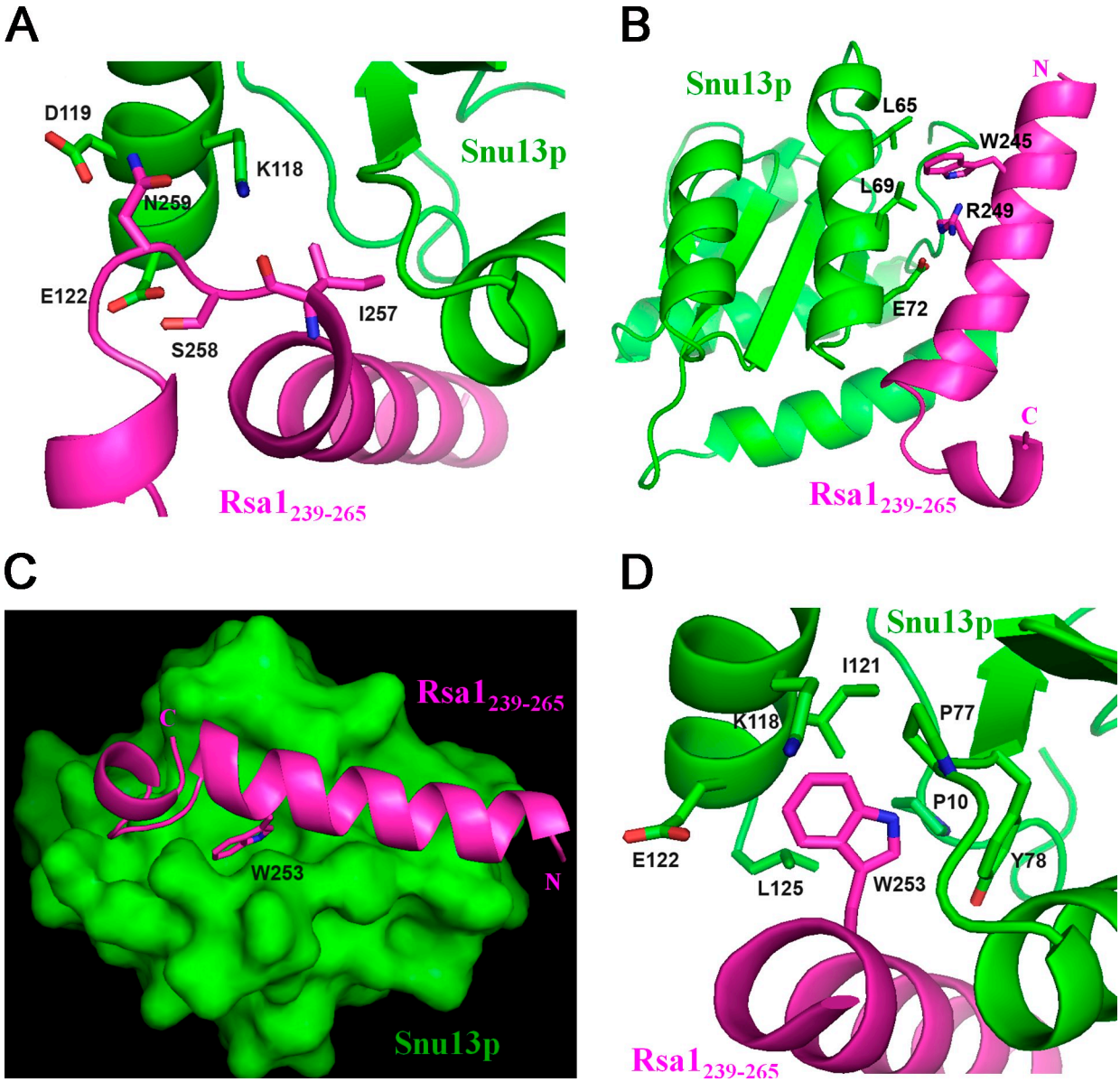

Figure 8. **Hydrogen bonds, ionic interaction, and hydrophobic contacts at the Snu13p–Rsa1p interface.** (A) Network of hydrogen bonds between Snu13p and Rsa1p. (B) Hydrophobic contacts and ionic interaction between Snu13p and Rsa1p. (C and D) The residue W253 of Rsa1p tightly binds in a hydrophobic pocket at the molecular surface of Snu13p.

structural biology approaches, we propose an assembly pathway that has three main features: (1) a protein-only complex that preassembles Nop58 and 15.5K, (2) the robust presence of RuvBL1/2, but not the other components of the R2TP complex, throughout most of the assembly pathway, and (3) the incompatibility between the presence of NUFIP and the formation of a catalytically active snoRNP structure.

ZNHIT3 and HIT Zn-finger proteins display tight links with RuvBL proteins

Using hBCD1 and NUFIP as baits, our proteomic experiments have identified ZNHIT3 as a new C/D snoRNP assembly factor. This protein is conserved across evolution, appears to interact directly with NUFIP, and forms a protein-only complex containing Nop58, 15.5K, NUFIP, hBCD1, RuvBL1, and RuvBL2. Such a preassembly of snoRNP proteins differs significantly from scenarios derived from in vitro experiments, from which a sequential recruitment of core proteins was proposed (Watkins et al., 2002; Schultz et al., 2006). Interestingly, although we did not detect association of ZNHIT3 with wild-type U3 snoRNA, we found that it bound well to a mutant form of U3 that carries three point mutations in stem II of the box C′/D motif. This mutant was previously shown to bind 15.5K but is impaired in its ability to form a complete C/D snoRNP because of missing contacts with Nop58 (Watkins et al., 2002; Ye et al., 2009; Xue et al., 2010). This suggests that the protein-only complex can bind RNA through 15.5K and that proper binding of Nop58 to the C/D motif triggers the release of ZNHIT3.

It is interesting to note that HIT Zn-finger proteins appear to have evolved specific links with the AAA^+ ATPases RuvBL1/2.

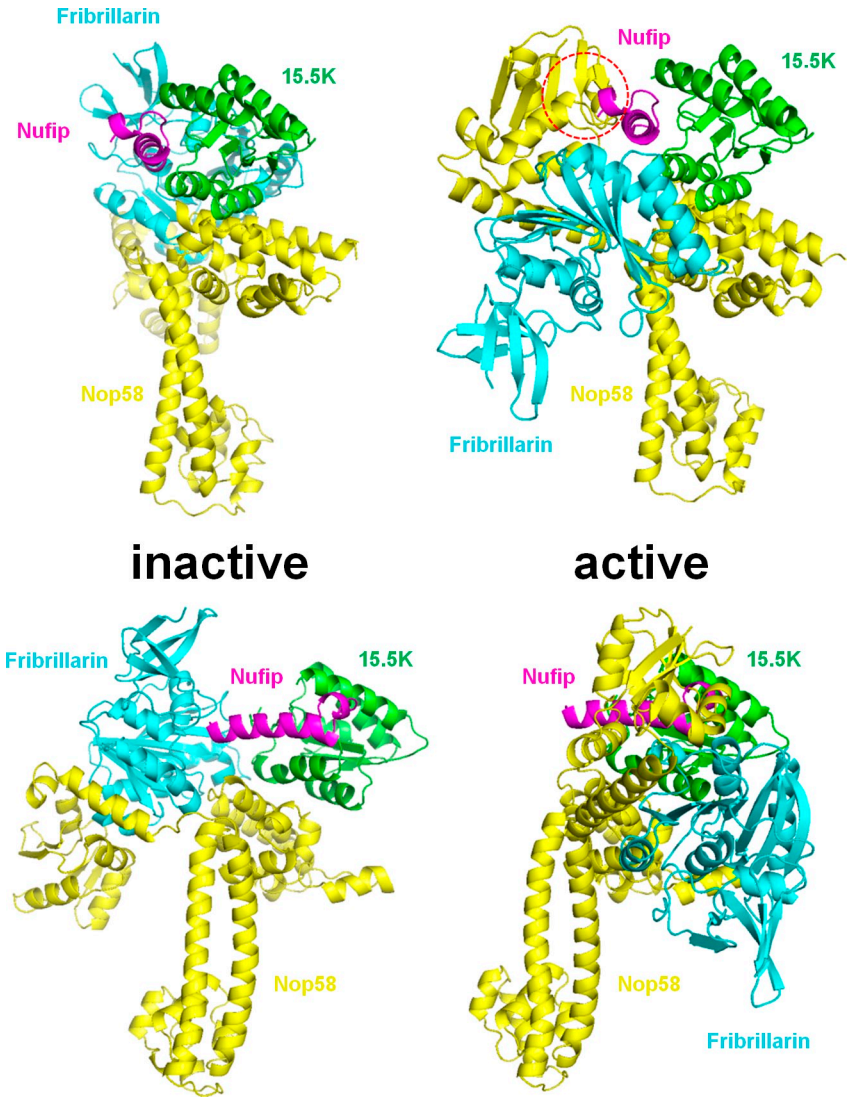

Figure 9. **Binding of Rsa1p to Snu13p prevents formation of the catalytically active structure of box C/D snoRNP.** Model of the human box C/D snoRNP comprising the core proteins 15.5K, Nop58, and Fibrillarin in inactive (left) and active (right) states. Both states were shown in two orthogonal views (up and down representations). The PEP domain of the protein factor NUFIP is represented in magenta. Whereas the presence of $NUFIP_{233–258}$ is compatible with the structure of the inactive form (comprising Nop58, Fibrillarin, and 15.5K), the rotation of the catalytic module of the box C/D snoRNP (including Fibrillarin and the N-terminal domain of Nop58) leads to a clash between the second α helix of $NUFIP_{233–258}$ and the N-terminal domain of Nop58. The region of spatial hindrance between NUFIP and Nop58 is indicated with a red dashed circle. Model was built on the basis of the known 3D structures of the box C/D sRNP in an inactive state from *P. furiosus* ((Xue et al., 2010); PDB no. 3NMU), in an active state from *S. solfataricus* (Lin et al., 2011; PDB no. 3PLA), and the crystal structure of $Snu13p–Rsa1_{239–265}$ (our work). The snoRNA is not depicted on these pictures.

There are six such proteins in the human genome (ZNHIT1–6). Two of them are involved in snoRNP biogenesis and are tightly associated with RuvBL1/2 in cells (ZNHIT3 and hBcd1/ZNHIT6; this study). Two other HIT Zn-finger proteins, ZNHIT1 and ZNHIT4, are part of the chromatin remodeling complexes SRCAP and Ino80, respectively, and RuvBL1/2 are also key components of these complexes. In addition, recent structural data of the yeast Ino80 complex indicates that the orthologue of ZNHIT4, Ies2p, makes many direct contacts with RuvBL1/2 and plays a central role in connecting them to the rest of the complex (Tosi et al., 2013). The remaining HIT Zn-finger proteins, ZNHIT2 and ZNHIT5/DDX59, are poorly characterized, but ZNHIT2 has also been found to be tightly associated with RuvBL proteins (Jeronimo et al., 2007). Collectively, these data thus suggest that ZNHIT proteins may contribute to the substrate specificity of RuvBL1/2. In addition, because hBCD1/ZNHIT6 makes ATP-dependent contact with RuvBL1/2 (McKeegan et al., 2009), and because ZNHIT3 appears to be released upon binding of the pre-snoRNP complex to snoRNAs, it is tempting to speculate that HIT Zn-finger proteins may play a particularly important role in the regulation of the activity and function of the RuvBL 1/2 proteins.

An assembly pathway for box C/D snoRNP points to the role of NUFIP in controlling snoRNP catalytic activity

Our structural data suggest that binding of NUFIP to the 15.5K protein prevents formation of the catalytically active snoRNP structure, and our proteomic and RNA binding experiments indicate that NUFIP remains bound to pre-snoRNPs until late stages of maturation. This indicates that one function of NUFIP is likely to prevent premature activation of the snoRNP catalytic activity. This is also reminiscent of H/ACA snoRNPs. In this case, the pre-snoRNPs contain Naf1 instead of Gar1. Naf1 is a structural homologue of Gar1 but it lacks a C-terminal domain that is required for substrate turnover (Li et al., 2011b). Similar cases also occur during ribosome maturation (Kemmler et al., 2009), and inhibition of the activity of immature noncoding RNP particles thus appears to be a general strategy during RNP biogenesis.

Collectively, our proteomic experiments and binding studies on U3 snoRNA allows us to propose an assembly scheme for box C/D snoRNPs (Fig. 10). It has three intermediates. First, a protein-only complex that contains ZNHIT3, NUFIP, hBCD1, and RuvBL1/2 associated with 15.5K and Nop58. Second, a box

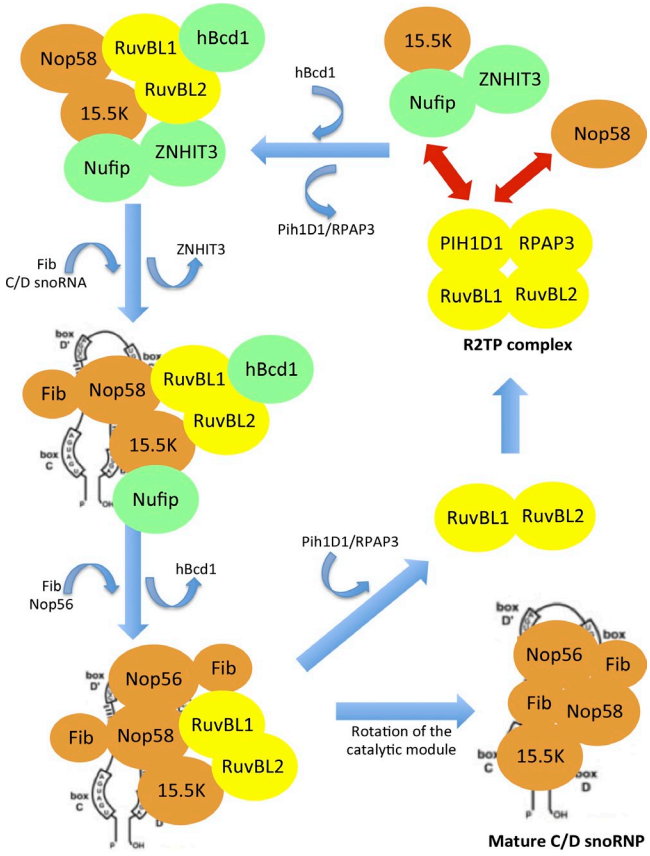

Figure 10. **An assembly scheme for human box C/D snoRNPs.** Complexes identified in the SILAC experiments were ordered according to the presence or absence of RNA and the presence of increasing numbers of core snoRNP proteins. The putative role of the R2TP complex is represented. Fib, Fibrillarin.

C/D snoRNA is incorporated to the nascent particle, and Fibrillarin interacts with Nop58. During this stage, the protein factor ZNHIT3 is released, whereas NUFIP is still bound to 15.5K to prevent the snoRNP from becoming catalytically active. Finally, Nop56 interacts with Nop58, whereas hBCD1 and NUFIP are released. The large rotation of the catalytic module (Fibrillarin and the N-terminal domain of Nop58) allowed by the release of NUFIP then leads to an active closed form of the box C/D snoRNP. In this closed configuration, the Nop58/Fibrillarin dimer interacts with the tip domain of Nop56 as well as with the snoRNA to direct 2′-*O*-methylation of the RNA target. Thus, Nop56 would play a major role in locking and stabilizing the box C/D snoRNP in a closed active configuration.

The R2TP complex: A role in loading/unloading RuvBL 1/2 proteins?

RuvBL1/2 are AAA$^+$ ATPases that play an essential role during snoRNP formation (King et al., 2001). In agreement, our proteomic and IP analyses indicate that they are present throughout the entire assembly pathway of box C/D snoRNPs. The R2TP complex is also involved in snoRNP biogenesis and contains the PIH1D1–RPAP3 heterodimer in addition to RuvBL1/2 (Pih1p and Tah1p in yeast; Zhao et al., 2005; Boulon et al., 2008; Eckert et al., 2010). However, our proteomic analysis failed to identify either PIH1D1, or RPAP3, in any of the pre-snoRNP complexes found. Interestingly, RuvBL1/2 have been shown to make mutually exclusive ATP-dependent contacts with hBCD1 and PIH1D1: they bind hBCD1 when loaded with ATP and PIH1D1 in the absence of nucleotides (McKeegan et al., 2009; Cheung et al., 2010). This mutually exclusive binding nicely correlates with our proteomic data: hBCD1, but not PIH1D1–RPAP3, is present in most of the pre-snoRNP complexes, whereas PIH1D1–RPAP3, but not hBCD1, is present in the R2TP–prefoldin-like complex. This would suggest that RuvBL1/2 are not bound to ATP when present within R2TP and are ATP loaded in pre-snoRNP complexes and thus unable to bind the PIH1D1–RPAP3 heterodimer.

One interesting hypothesis for the role of the R2TP would thus be that it loads/unloads RuvBL1/2 proteins on target complexes in an ATP-dependent manner (Fig. 10). Interestingly, PIH1D1 interacts with both Nop58 and NUFIP (Gonzales et al., 2005; Boulon et al., 2008; Zhao et al., 2008), and NUFIP can itself form a separate ternary complex with 15.5K and ZNHIT3 (Boulon et al., 2008; this work and our unpublished data). The PIH1D1–RPAP3 dimer bound to RuvBL1/2 might thus connect Nop58 to the ZNHIT3–NUFIP–15.5K ternary complex and may stimulate the ATP-dependent transfer of the RuvBL proteins from the R2TP to pre-snoRNPs, which would generate the protein-only, ZNHIT3 complex. In agreement with such a role of the R2TP complex, we found that yeast Nop58p mutants unable to interact with Snu13p/15.5K and to assemble into a snoRNP interact more strongly with both Pih1p and Tah1p by two-hybrid assays (Fig. S4 C).

A role for the R2TP in loading and unloading the RuvBL proteins would explain why several complexes that contain these proteins lack PIH1D1 and RPAP3. This would suggest that many of these complexes, and in particular Ino80 and Swr1, are in fact clients of the HSP90–R2TP chaperone complex, with some of their subunits passing from HSP90 to RuvBL 1/2 via R2TP.

Materials and methods

Plasmids, cell lines, and antibodies

HeLa, U2OS, and 293T cells were cultivated in DMEM with antibiotics and 10% FCS. Stable U2OS cells lines were obtained by cotransfecting the GFP-expressing plasmid with a pCMV-Hygro selection plasmid. Clones were selected on 50 mM hygromycin B (EMD Millipore), picked, expended individually, and characterized by Western blots and by GFP fluorescence microscopy. Stable isogenic 293T cells expressing the GST-tagged proteins were obtained with 293T Flp-In cells, by cotransfecting the parental cells with pcDNA5-GST-NUFIP and pcDNA5-GST-ZNHIT3 and a Flippase expression vector with Lipofectamine and Plus reagent (Invitrogen). Stable clones were then selected with hygromycin B and processed as U2OS clones. Individual clones usually expressed similar levels of the tagged protein. DNA cloning was performed by standard techniques and with the Gateway system (Invitrogen). Antibodies and dilutions for Western blots were the following: rabbit polyclonal anti–human NUFIP (Proteintech Group) at 1:1,000, rabbit polyclonal anti–human ZNHIT3 (Abcam) at 1:5,000, rabbit polyclonal anti–human RuvBL1 (Proteintech Group) at 1:1,000, rabbit polyclonal anti–human RuvBL2 (Proteintech Group) at 1:1,000, rabbit polyclonal anti-Nop58 raised against the N-terminal region of human Nop58 (residues 20–37; Eurogentec) at 1:2,000, and rabbit polyclonal anti-GFP (Molecular Probes) at 1:8,000.

IP and RNA analyses

Cells were extracted in HNTG buffer (20 mM Hepes, pH 7.9, 150 mM NaCl, 1% Triton X-100, 10% glycerol, 1 mM $MgCl_2$, 1 mM EGTA, and protease inhibitors) for 30 min at 4°C. Cellular debris were removed by

centrifugation (10 min at 9,000 *g*). Extracts were put on antibody-coated beads for 2 h at 4°C (GFP-TRAP for GFP, obtained from ChromoTek; glutathione beads for GST, obtained from GE Healthcare). Beads were washed twice in HNTG and three times in PBS, and pelleted materials were homogenized in TRIZOL (Invitrogen). RNAs were purified according to the manufacturer's instructions. RNase protection assays were performed with RNAPIII kit (Ambion), with ^{32}P-labeled probes spanning the 3′ end of rat U3 snoRNA covering nucleotides 98–236 of rU3B.7 (1 is first nucleotide of mature U3; Verheggen et al., 2002).

Fluorescence microscopy, image acquisition, and quantification

Cells were grown on coverslips, washed in PBS, and fixed in 4% (wt/vol) formaldehyde in PBS at RT (for 20 min) followed by permeabilization either with 0.1% Triton X-100 in PBS for 5 min at RT for antibody labeling or with ethanol 70%, overnight at 4°C for in situ hybridizations, which were performed with Cy3-labeled oligonucleotides against rat U3 as previously described (Verheggen et al., 2002). Coverslips were mounted on glass slides using mounting medium (Vectashield), and samples were observed at RT using a fluorescence microscope (100×, NA 1.4; DMRA; Leica). Images were acquired with a camera (CoolSNAP HQ2; Princeton Instrument) using MetaMorph (Molecular Devices) and processed with Photoshop (Adobe).

In vitro GST pull-downs

GST-Hit1p was expressed in *Escherichia coli* BL21(DE3) and purified on glutathione beads. Radiolabeled Rsa1p protein was synthesized in the presence of [^{35}S]methionine in rabbit reticulocyte lysate (TNT; Promega). Binding was performed with 5 µg GST-Hit1p in 20 mM Tris-HCl, pH 8, 40 mM KCl, 1 mM $MgCl_2$, 0.1 mM EDTA, 0.1% NP-40, and 10% glycerol. Washing was performed with the same buffer but with 100 mM KCl instead of 40 mM and 5 mM $MgCl_2$ instead of 1 mM. Gels were transferred to membranes and subjected to autoradiography.

Yeast two-hybrid assays

Appropriate pACT2 and pAS2ΔΔ plasmids were introduced into haploid *Saccharomyces cerevisiae* test strains (CG1945 and Y187, respectively), which were then crossed. Diploids were selected on −Leu −Trp media and then plated on test plates lacking Leu, Trp, and His. This was used to evaluate the strength of the interactions. Growth was assessed after 3 d of incubation at 30°C. The score is then given by comparing the number of diploid clones growing on −L −T (selections of diploids) and −L −T −H plates (selection for interaction).

SILAC proteomic analysis

SILAC experiments were performed as previously described (Boulon et al., 2010b). Cells were grown in custom-made DMEM (minus arginine and lysine; Invitrogen) supplemented with 10% dialyzed FCS (Biowest) and penicillin-streptomycin (Invitrogen). L-arginine and L-lysine (Sigma-Aldrich) were added to the "light," L-arginine ^{13}C and L-lysine 4,4,5,5-D4 (Eurositop) were added to the "medium," and L-arginine ^{13}C/^{15}N and L-lysine ^{13}C/^{15}N (Eurositop) were added to the "heavy" media. The amino acid concentrations were based on the formula for normal DMEM (Invitrogen). U2OS cells were grown for 10 d in each isotopically labeled media to ensure complete incorporation of isotopic amino acids and treated with the indicated drugs at 75% confluence for the last 14 h. Five 15-cm diameter plates were used per SILAC condition. Cells were rinsed with PBS at 4°C, trypsinized, and extracted a first time for 10 min at 4°C in 20 mM Tris HCl, pH 7.5, 10 mM KCl, 3 mM $MgCl_2$, 0.1% NP-40, 10% glycerol, and Complete antiprotease cocktail (Roche). After centrifugation at 750 *g* for 10 min, pellets were extracted a second time 4°C in 50 mM Tris HCl, pH 7.5, 150 mM NaCl, 1% NP-40, 0.5% deoxycholate, and Complete antiprotease cocktail and sonicated for 3 × 10 s. Extracts were cleared by centrifugation at 2,800 *g* for 10 min at 4°C to remove cellular debris. An aliquot of each extract was kept and subjected to Western blotting to verify the action of the drugs. The first extraction corresponded to the more extractable fraction, and the second extraction was the less extractable fraction. When indicated, extracts were treated with 0.6 µg/ml RNase A. For all IP experiments, extracts were precleared by incubation on protein G Sepharose beads (GE Healthcare) for 1 h at 4°C. Extracts labeled with light, medium, and heavy amino acids were pooled in a 1:1:1 ratio based on total protein concentration and incubated with GFP-TRAP beads for 2 h at 4°C. The control, light extracts originated from parental cells that did not express the GFP fusion. After the affinity purification step, beads were washed five times with the extraction buffer. Bound proteins were eluted by adding 1% SDS to the beads and boiling for 10 min. Samples were then reduced with 10 mM DTT (BDH Chemicals) at 95°C for 2 min and alkylated using 50 mM iodoacetamide (Sigma-Aldrich) for 30 min. Proteins were separated on 1D SDS/PAGE, the lanes of interest were cut in 10 slices, and proteins were in-gel digested by trypsin in 20 mM NH_4HCO_3 (Trypsin Gold; Promega). Peptides were extracted from gel pieces, dried, and resuspended in 0.1% formic acid solution for analysis on a mass spectrometer (Orbitrap Elite Hybrid Ion Trap; Thermo Fisher Scientific) coupled to a nanoflow liquid chromatography system (UltiMate U3000; Thermo Fisher Scientific). One tenth of each band digest was loaded onto a PepMap C18 trap column (0.3-mm inner diameter × 5 mm; Dionex Corporation) with a constant flow of 20 µl/min. After trap enrichment peptides, a gradient consisting of 2–40% buffer B (3–33 min), 40–80% B (33–34 min), 80–0% B (49–50 min), and equilibrated for 20 min in 0% B (50–70 min) was used to elute peptides at 300 nl/min from a PepMap capillary (0.075 mm × 150 mm) reversed-phase column (LC Packings). Mass spectra were acquired using a top-20 collision-induced dissociation data-dependent acquisition method. The LTQ-Orbitrap was programmed to perform a Fourier transform (FT) full scan (60,000 resolution) on 400–1,400-Th mass range with the top 20 ions from each scan selected for LTQ-MS/MS. FT spectra were internally calibrated using a single lock mass (445.1200 Th). Target ion numbers were 500,000 for FT full scan on the Orbitrap and 10,000 MS2 on the LTQ. Quantitation was performed using the program MaxQuant (version 1.4.1.2; Cox et al., 2009) and with the Mascot search engine (version 2.1.04; Matrix Science). Enzyme specificity was set to that of trypsin, allowing for cleavage N-terminal to proline residues and between aspartic acid and proline residues. Other parameters used were (a) variable modifications: methionine oxidation and protein *N*-acetylation; (b) fixed modifications: cysteine carbamidomethylation; (c) database: target decoy human MaxQuant; (d) heavy labels: R6K4 and R10K8; (e) MS/MS tolerance: 0.5 D; (f) maximum peptide length: 6; (g) top MS/MS peaks per 100 D: 6; (h) maximum missed cleavages: 2; (i) maximum of labeled amino acids: 3; and (j) false discovery rate: 5%. In addition to the false discovery rate, proteins were considered to be identified if they had at least one unique peptide, and they were considered quantified if they had at least one quantified SILAC pair, although the number of unique peptides and the number of ratio counts were taken into account during the analysis process to assess the reliability of protein identification and quantification. Proteins labeled as REV (nonreal proteins from the reverse database) were automatically discarded, as well as proteins that did not show any SILAC medium/light, heavy/light, and heavy/medium ratio. SILAC ratios were normalized so that the median enrichment of the specific IP over the control, mostly caused by contaminant proteins, was one. Keratins were removed, and proteins were considered as hits if they had a SILAC ratio (specific IP/control IP) >3.5 or if their SILAC ratio was between 1.5 and 3.5 but with a frequency of detection in unrelated IPs of <25% (Boulon et al., 2010a). The network graph was created with Cytoscape, using the hit list of Table S3, filtered to retain only proteins with a role in snoRNP biogenesis. In a second analysis, we used a clustering algorithm to group proteins from all the SILAC performed. To do so, the hit list was filtered to remove all the proteins found only once. Clustering was performed using the EPCLUST server (http://www.bioinf.ebc.ee/EP/EP/EPCLUST), using complete linkage (maximum distance) clustering based on linear correlation–based distance (Pearson, centered). Similar protein groups were obtained using *k*-means (eight clusters, correlation-based distance). For the time-resolved SILAC proteomic experiment, GFP-Nop58 was transiently expressed in HeLa cells for 10 h or stably expressed. These cells and control, untransfected cells were isotopically labeled and extracted by cryogrinding, GFP-Nop58 was pulled down using GFP-TRAP beads, and associated proteins were identified by MS. SILAC ratios of the specific versus control IP were normalized by first subtracting the mean ratios of all proteins identified and then by dividing by the ratio found for GFP-Nop58.

Protein overexpression, purification, and crystallization

We did not succeed to get crystals suitable for x-ray analysis with the human proteins or when complexes were formed with the previously identified yeast PEP region (residues 230–266 of Rsa1p). However, after several trials, we found that a slightly larger fragment of yeast PEP (residues 238–290 of Rsa1p) formed a stable complex with full-length Snu13p and gave high quality crystals after purification to homogeneity. For preparation of recombinant protein, the coding sequence of yeast Snu13p ORF and the yeast Rsa1$_{238–290}$ fragment from *S. cerevisiae* were PCR amplified and cloned into the expression vectors pnEA-3CH and pnCS, respectively (Diebold et al., 2011). *E. coli* BL21(DE3)pRARE2 cells cotransformed with both plasmids were grown at 37°C to an A_{600} of 0.7 in 1 liter of 2YT medium containing 100 µg/ml ampicillin and 30 µg/ml spectinomycin. Protein expression was induced by addition of 0.2 mM isopropyl-β-D-thiogalactopyranoside,

and growth was continued overnight at 20°C. For purification of the His6–Snu13p–Rsa1$_{238–290}$ complex, cells were sonicated in buffer A (25 mM Hepes, pH 7.5, 400 mM NaCl, 5 mM 2-mercaptoethanol, and 10 mM imidazole). After 30 min centrifugation at 4°C and 12,000 *g*, nucleic acids from the supernatant were precipitated by addition of 0.0125% polyethylenimine. A second centrifugation was performed for 20 min at 12,000 *g*, and the supernatant was directly incubated with TALON Superflow Metal Affinity Resin (Takara Bio Inc.). The beads were then successively washed with buffer A and buffer B (25 mM Hepes, pH 7.5, 300 mM NaCl, and 5 mM 2-mercaptoethanol). Elimination of the His tag by proteolytic cleavage was directly performed on the beads in buffer B overnight at 4°C, using the PreScission protease (GE Healthcare). The protein complex was further purified to homogeneity by Superdex 75 gel filtration chromatography using buffer C (10 mM Hepes, pH 7.5, and 150 mM NaCl) and concentrated by the use of a 15-ml system (10-kD cutoff; Amicon Ultra; EMD Millipore) to 56 mg/ml final concentration. A His6–Snu13p–Rsa1$_{238–290}$ Se-Met protein complex was overexpressed in *E. coli* B834(DE3) (Met auxotroph) and purified as described for purification of the His6–Snu13p–Rsa1$_{238–290}$ complex.

Crystals of the Snu13p–Rsa1$_{238–290}$ complex were obtained by vapor phase diffusion and grew in mother liquor containing 2.3 M ammonium sulfate and 70 mM sodium citrate buffer, pH 5.0. Drops were made at 20°C by mixing 1 µl of the concentrated proteins mixture (56 mg/ml) and 1 µl of the reservoir solution. The crystals were in space group $P4_32_12$ with unit cell parameters a = 59.7 Å, b = 59.7 Å, and c = 92.5 Å, and assuming one protein complex in the asymmetric unit, the packing density V_M is 1.99 Å^3/D, and the solvent content is 38.3%. Crystals of Se-Met–incorporated proteins were obtained under conditions similar to those used for the wild-type complex.

Diffraction data collection and crystal structure determination

Crystals were flash frozen in liquid nitrogen in the mother liquor with addition of 20% glycerol as a cryoprotectant. A native dataset at 1.55-Å resolution was collected at 100 K on beamline ID14-4 at the European Synchrotron Radiation Facility, with incident radiation at a wavelength of 0.980 Å and a crystal-to-detector distance of 243 mm. Diffraction spots were recorded on a charge-coupled device detector (Q315r; ADSC) with a 1° oscillation and a 0.2-s exposure per charge-coupled device image over a range of 360°. Data were indexed and scaled using XDS (Kabsch, 2010). Indexed intensities were converted to structure factors using TRUNCATE in the CCP4 suite (Winn et al., 2011) without any σ cutoff.

The single anomalous diffraction data from Se-Met Snu13p–Rsa1$_{238–290}$ crystals were collected at absorption peak up to 1.9-Å resolution at the ID14-4 beamline at European Synchrotron Radiation Facility. The dataset was indexed and scaled using XDS (Kabsch, 2010). Three over six possible selenium sites were found and refined at 2.5-Å resolution using SOLVE (Terwilliger and Berendzen, 1999), which produced a mean figure of merit of 0.48 and an overall score of 18. After density modification with RESOLVE (Terwilliger, 2000), the mean figure of merit was 0.77. Building of the model was performed using Coot (Emsley et al., 2010), and the refinement of the crystal structure was performed in the range 40–1.55 Å using REFMAC5 (Vagin et al., 2004) with TLS (translation/libration/screw) parameters (two TLS groups). A total of 5% of the native data were selected for R_{free} calculations. The model was refined to the final R_{factor} of 19.6% and R_{free} of 23.2% (Table S2). The asymmetric unit contains one Snu13p–Rsa1$_{238–290}$ complex, 95 water molecules, and one sulfate ion. Because of the lack of density, residues 1–3 and 126 of Snu13p and residues 238 and 266–290 of Rsa1p were not built. They were probably too flexible in the complex to generate a clear electron density. Coordinates of the Snu13p–Rsa1$_{238–265}$ structure have been submitted to the PDB. Over 94% of the residues were within the most favored regions, and no residue was within the disallowed regions in a Ramachandran plot, as defined by PROCHECK (Laskowski et al., 1993). Averaged B factors were of 26.2 Å^2 for the protein atoms, 31.5 Å^2 for water molecules, 22.9 Å^2 for the sulfate ion, and 26.5 Å^2 for the whole structure.

Homology modeling of human snoRNP C/D

To build the models of the human snoRNP C/D in active and inactive states, we used the crystal structures of the box C/D sRNP in an inactive state from *Pyrococcus furiosus* (Xue et al., 2010; PDB 3NMU) and in an active state from *Sulfolobus solfataricus* (Lin et al., 2011; PDB 3PLA) as well as the crystal structure of Snu13p–Rsa1$_{239–265}$ (our work). Models of the human box C/D snoRNP comprise the protein factor NUFIP$_{233–258}$ and the core proteins 15.5K (PDB 1E7K), Nop58, and Fibrillarin that were obtained using the program Modeller (Eswar et al., 2006) with the crystal structures of homologous proteins. The assembly of the human snoRNPs was achieved by applying several steps of least-squares superimpositions of backbone atoms in accordance with the crystal structures of archaeal complexes.

Online supplemental material

Fig. S1 shows interactions between snoRNP assembly factor and C/D core proteins that were tested by IP and Western blot, two-hybrid assays, and in vitro GST pull-down. Fig. S2 shows a plot for two SILAC-IP of ZNHIT3 (with and without RNase) to reveal the RNase-independent interactions of ZNHIT3 and also shows yeast two-hybrid assays with c12orf45 and time-resolved SILAC-IP of GFP-Nop58. Fig. S3 shows that single and continuous surface of Snu13p is buried upon interaction with the PEP domain of Rsa1p. Fig. S4 shows a comparison of yeast Snu13p–Rsa1p with human 15.5K-NUFIP to reveal conservation of residues involved in the interface and also shows a table of two-hybrid assays performed with yeast Nop58p mutants revealing a stronger interaction with Pih1p and Tah1p for Nop58p mutant K311A A314R, which specifically loose interaction with Snu13p. Table S1 shows nomenclature used in this study. Table S2 shows crystallographic statistics. Table S3 shows a hit list of the proteomic experiments and is available online as an Excel file. Online supplemental material is available at http://www.jcb.org/cgi/content/full/jcb.201404160/DC1. Additional data are available in the JCB DataViewer at http://dx.doi.org/10.1083/jcb.201404160.dv.

We thank the Functional Proteomic Platform of Montpellier (France), the Service Commun de Biophysicochimie des Interactions Moléculaires (Université de Lorraine), and the FR3209 Ingénierie Moléculaire et Thérapeutique for the use of their instruments. We are grateful to the European Synchrotron Radiation Facility for access to the ID14-4 beamline.

This work was supported by the Centre de la Recherche Scientifique, University of Lorraine, the Agence Nationale de la Recherche (ANR; grant no. ANR-11-BSV8-01503), grants from La Ligue contre le Cancer (équipe labellisée grant #30025555 Grand-Est), Association de la Recherche contre le Cancer (ARC), the Pôle de Recherche Scientifique et Technologique de la Région Lorraine, the European Associated Laboratory on pre-mRNA splicing (Centre National de la Recherche Scientifique, Lorraine University, Montpellier University, and the Max Planck Institute), and the Fondation pour la Recherche Médicale. J. Bizarro was supported by fellowships from the French Research Ministry and from the ARC. A. Lamond is a Wellcome Trust Principal Research Fellow.

The authors declare no competing financial interests.

Submitted: 30 April 2014
Accepted: 20 October 2014

References

Aittaleb, M., R. Rashid, Q. Chen, J.R. Palmer, C.J. Daniels, and H. Li. 2003. Structure and function of archaeal box C/D sRNP core proteins. *Nat. Struct. Biol.* 10:256–263. http://dx.doi.org/10.1038/nsb905

Back, R., C. Dominguez, B. Rothé, C. Bobo, C. Beaufils, S. Moréra, P. Meyer, B. Charpentier, C. Branlant, F.H. Allain, and X. Manival. 2013. High-resolution structural analysis shows how Tah1 tethers Hsp90 to the R2TP complex. *Structure*. 21:1834–1847. http://dx.doi.org/10.1016/j.str.2013.07.024

Bardoni, B., A. Schenck, and J.L. Mandel. 1999. A novel RNA-binding nuclear protein that interacts with the fragile X mental retardation (FMR1) protein. *Hum. Mol. Genet.* 8:2557–2566. http://dx.doi.org/10.1093/hmg/8.13.2557

Battle, D.J., C.K. Lau, L. Wan, H. Deng, F. Lotti, and G. Dreyfuss. 2006. The Gemin5 protein of the SMN complex identifies snRNAs. *Mol. Cell*. 23:273–279. http://dx.doi.org/10.1016/j.molcel.2006.05.036

Boulon, S., C. Verheggen, B.E. Jady, C. Girard, C. Pescia, C. Paul, J.K. Ospina, T. Kiss, A.G. Matera, R. Bordonné, and E. Bertrand. 2004. PHAX and CRM1 are required sequentially to transport U3 snoRNA to nucleoli. *Mol. Cell*. 16:777–787. http://dx.doi.org/10.1016/j.molcel.2004.11.013

Boulon, S., N. Marmier-Gourrier, B. Pradet-Balade, L. Wurth, C. Verheggen, B.E. Jády, B. Rothé, C. Pescia, M.C. Robert, T. Kiss, et al. 2008. The Hsp90 chaperone controls the biogenesis of L7Ae RNPs through conserved machinery. *J. Cell Biol.* 180:579–595. http://dx.doi.org/10.1083/jcb.200708110

Boulon, S., Y. Ahmad, L. Trinkle-Mulcahy, C. Verheggen, A. Cobley, P. Gregor, E. Bertrand, M. Whitehorn, and A.I. Lamond. 2010a. Establishment of a protein frequency library and its application in the reliable identification of specific protein interaction partners. *Mol. Cell. Proteomics*. 9:861–879. http://dx.doi.org/10.1074/mcp.M900517-MCP200

Boulon, S., B. Pradet-Balade, C. Verheggen, D. Molle, S. Boireau, M. Georgieva, K. Azzag, M.C. Robert, Y. Ahmad, H. Neel, et al. 2010b. HSP90 and its R2TP/Prefoldin-like cochaperone are involved in the cytoplasmic assembly of RNA polymerase II. *Mol. Cell*. 39:912–924. http://dx.doi.org/10.1016/j.molcel.2010.08.023

Cavaillé, J., M. Nicoloso, and J.P. Bachellerie. 1996. Targeted ribose methylation of RNA in vivo directed by tailored antisense RNA guides. *Nature*. 383:732–735. http://dx.doi.org/10.1038/383732a0

Chari, A., M.M. Golas, M. Klingenhäger, N. Neuenkirchen, B. Sander, C. Englbrecht, A. Sickmann, H. Stark, and U. Fischer. 2008. An assembly chaperone collaborates with the SMN complex to generate spliceosomal SnRNPs. *Cell*. 135:497–509. http://dx.doi.org/10.1016/j.cell.2008.09.020

Charron, C., X. Manival, B. Charpentier, C. Branlant, and A. Aubry. 2004a. Purification, crystallization and preliminary X-ray diffraction data of L7Ae sRNP core protein from *Pyrococcus abyssii*. *Acta Crystallogr. D Biol. Crystallogr.* 60:122–124. http://dx.doi.org/10.1107/S090744490302239X

Charron, C., X. Manival, A. Cléry, V. Senty-Ségault, B. Charpentier, N. Marmier-Gourrier, C. Branlant, and A. Aubry. 2004b. The archaeal sRNA binding protein L7Ae has a 3D structure very similar to that of its eukaryal counterpart while having a broader RNA-binding specificity. *J. Mol. Biol.* 342:757–773. http://dx.doi.org/10.1016/j.jmb.2004.07.046

Cheung, K.L., J. Huen, Y. Kakihara, W.A. Houry, and J. Ortega. 2010. Alternative oligomeric states of the yeast Rvb1/Rvb2 complex induced by histidine tags. *J. Mol. Biol.* 404:478–492. http://dx.doi.org/10.1016/j.jmb.2010.10.003

Cloutier, P., R. Al-Khoury, M. Lavallée-Adam, D. Faubert, H. Jiang, C. Poitras, A. Bouchard, D. Forget, M. Blanchette, and B. Coulombe. 2009. High-resolution mapping of the protein interaction network for the human transcription machinery and affinity purification of RNA polymerase II-associated complexes. *Methods*. 48:381–386. http://dx.doi.org/10.1016/j.ymeth.2009.05.005

Cox, J., I. Matic, M. Hilger, N. Nagaraj, M. Selbach, J.V. Olsen, and M. Mann. 2009. A practical guide to the MaxQuant computational platform for SILAC-based quantitative proteomics. *Nat. Protoc.* 4:698–705. http://dx.doi.org/10.1038/nprot.2009.36

Diebold, M.L., S. Fribourg, M. Koch, T. Metzger, and C. Romier. 2011. Deciphering correct strategies for multiprotein complex assembly by co-expression: application to complexes as large as the histone octamer. *J. Struct. Biol.* 175:178–188. http://dx.doi.org/10.1016/j.jsb.2011.02.001

Eckert, K., J.M. Saliou, L. Monlezun, A. Vigouroux, N. Atmane, C. Caillat, S. Quevillon-Chéruel, K. Madiona, M. Nicaise, S. Lazereg, et al. 2010. The Pih1-Tah1 cochaperone complex inhibits Hsp90 molecular chaperone ATPase activity. *J. Biol. Chem.* 285:31304–31312. http://dx.doi.org/10.1074/jbc.M110.138263

Emsley, P., B. Lohkamp, W.G. Scott, and K. Cowtan. 2010. Features and development of Coot. *Acta Crystallogr. D Biol. Crystallogr.* 66:486–501. http://dx.doi.org/10.1107/S0907444910007493

Eswar, N., B. Webb, M.A. Marti-Renom, M.S. Madhusudhan, D. Eramian, M.Y. Shen, U. Pieper, and A. Sali. 2006. Comparative protein structure modeling using Modeller. *Curr. Protoc. Bioinformatics*. Chapter 5:Unit 5.6.

Fischer, U., Q. Liu, and G. Dreyfuss. 1997. The SMN-SIP1 complex has an essential role in spliceosomal snRNP biogenesis. *Cell*. 90:1023–1029. http://dx.doi.org/10.1016/S0092-8674(00)80368-2

Fischer, U., C. Englbrecht, and A. Chari. 2011. Biogenesis of spliceosomal small nuclear ribonucleoproteins. *Wiley Interdiscip. Rev. RNA*. 2:718–731. http://dx.doi.org/10.1002/wrna.87

Gonzales, F.A., N.I. Zanchin, J.S. Luz, and C.C. Oliveira. 2005. Characterization of *Saccharomyces cerevisiae* Nop17p, a novel Nop58p-interacting protein that is involved in Pre-rRNA processing. *J. Mol. Biol.* 346:437–455. http://dx.doi.org/10.1016/j.jmb.2004.11.071

Gorynia, S., T.M. Bandeiras, F.G. Pinho, C.E. McVey, C. Vonrhein, A. Round, D.I. Svergun, P. Donner, P.M. Matias, and M.A. Carrondo. 2011. Structural and functional insights into a dodecameric molecular machine - the RuvBL1/RuvBL2 complex. *J. Struct. Biol.* 176:279–291. http://dx.doi.org/10.1016/j.jsb.2011.09.001

Grimm, C., A. Chari, J.P. Pelz, J. Kuper, C. Kisker, K. Diederichs, H. Stark, H. Schindelin, and U. Fischer. 2013. Structural basis of assembly chaperone-mediated snRNP formation. *Mol. Cell*. 49:692–703. http://dx.doi.org/10.1016/j.molcel.2012.12.009

Grozdanov, P.N., S. Roy, N. Kittur, and U.T. Meier. 2009. SHQ1 is required prior to NAF1 for assembly of H/ACA small nucleolar and telomerase RNPs. *RNA*. 15:1188–1197. http://dx.doi.org/10.1261/rna.1532109

Ito, T., T. Chiba, R. Ozawa, M. Yoshida, M. Hattori, and Y. Sakaki. 2001. A comprehensive two-hybrid analysis to explore the yeast protein interactome. *Proc. Natl. Acad. Sci. USA*. 98:4569–4574. http://dx.doi.org/10.1073/pnas.061034498

Jeronimo, C., D. Forget, A. Bouchard, Q. Li, G. Chua, C. Poitras, C. Thérien, D. Bergeron, S. Bourassa, J. Greenblatt, et al. 2007. Systematic analysis of the protein interaction network for the human transcription machinery reveals the identity of the 7SK capping enzyme. *Mol. Cell*. 27:262–274. http://dx.doi.org/10.1016/j.molcel.2007.06.027

Kabsch, W. 2010. XDS. *Acta Crystallogr. D Biol. Crystallogr.* 66:125–132. http://dx.doi.org/10.1107/S0907444909047337

Kemmler, S., L. Occhipinti, M. Veisu, and V.G. Panse. 2009. Yvh1 is required for a late maturation step in the 60S biogenesis pathway. *J. Cell Biol.* 186:863–880. http://dx.doi.org/10.1083/jcb.200904111

King, T.H., W.A. Decatur, E. Bertrand, E.S. Maxwell, and M.J. Fournier. 2001. A well-connected and conserved nucleoplasmic helicase is required for production of box C/D and H/ACA snoRNAs and localization of snoRNP proteins. *Mol. Cell. Biol.* 21:7731–7746. http://dx.doi.org/10.1128/MCB.21.22.7731-7746.2001

Kiss, T., E. Fayet, B.E. Jády, P. Richard, and M. Weber. 2006. Biogenesis and intranuclear trafficking of human box C/D and H/ACA RNPs. *Cold Spring Harb. Symp. Quant. Biol.* 71:407–417. http://dx.doi.org/10.1101/sqb.2006.71.025

Kiss, T., E. Fayet-Lebaron, and B.E. Jády. 2010. Box H/ACA small ribonucleoproteins. *Mol. Cell*. 37:597–606. http://dx.doi.org/10.1016/j.molcel.2010.01.032

Kiss-László, Z., Y. Henry, J.P. Bachellerie, M. Caizergues-Ferrer, and T. Kiss. 1996. Site-specific ribose methylation of preribosomal RNA: a novel function for small nucleolar RNAs. *Cell*. 85:1077–1088. http://dx.doi.org/10.1016/S0092-8674(00)81308-2

Lapinaite, A., B. Simon, L. Skjaerven, M. Rakwalska-Bange, F. Gabel, and T. Carlomagno. 2013. The structure of the box C/D enzyme reveals regulation of RNA methylation. *Nature*. 502:519–523. http://dx.doi.org/10.1038/nature12581

Laskowski, R.A., M.W. McArthur, D.S. Moss, and J.M. Thornton. 1993. PROCHECK: a program to check the stereochemical quality of protein structures. *J. Appl. Cryst.* 26:283–291. http://dx.doi.org/10.1107/S0021889892009944

Li, S., J. Duan, D. Li, S. Ma, and K. Ye. 2011a. Structure of the Shq1-Cbf5-Nop10-Gar1 complex and implications for H/ACA RNP biogenesis and dyskeratosis congenita. *EMBO J.* 30:5010–5020. http://dx.doi.org/10.1038/emboj.2011.427

Li, S., J. Duan, D. Li, B. Yang, M. Dong, and K. Ye. 2011b. Reconstitution and structural analysis of the yeast box H/ACA RNA-guided pseudouridine synthase. *Genes Dev.* 25:2409–2421. http://dx.doi.org/10.1101/gad.175299.111

Liang, B., and H. Li. 2011. Structures of ribonucleoprotein particle modification enzymes. *Q. Rev. Biophys.* 44:95–122. http://dx.doi.org/10.1017/S0033583510000235

Lin, J., S. Lai, R. Jia, A. Xu, L. Zhang, J. Lu, and K. Ye. 2011. Structural basis for site-specific ribose methylation by box C/D RNA protein complexes. *Nature*. 469:559–563. http://dx.doi.org/10.1038/nature09688

Liu, S., P. Li, O. Dybkov, S. Nottrott, K. Hartmuth, R. Lührmann, T. Carlomagno, and M.C. Wahl. 2007. Binding of the human Prp31 Nop domain to a composite RNA-protein platform in U4 snRNP. *Science*. 316:115–120. http://dx.doi.org/10.1126/science.1137924

Lukowiak, A.A., S. Granneman, S.A. Mattox, W.A. Speckmann, K. Jones, H. Pluk, W.J. Venrooij, R.M. Terns, and M.P. Terns. 2000. Interaction of the U3-55k protein with U3 snoRNA is mediated by the box B/C motif of U3 and the WD repeats of U3-55k. *Nucleic Acids Res.* 28:3462–3471. http://dx.doi.org/10.1093/nar/28.18.3462

Machado-Pinilla, R., D. Liger, N. Leulliot, and U.T. Meier. 2012. Mechanism of the AAA+ ATPases pontin and reptin in the biogenesis of H/ACA RNPs. *RNA*. 18:1833–1845. http://dx.doi.org/10.1261/rna.034942.112

Matera, A.G., R.M. Terns, and M.P. Terns. 2007. Non-coding RNAs: lessons from the small nuclear and small nucleolar RNAs. *Nat. Rev. Mol. Cell Biol.* 8:209–220. http://dx.doi.org/10.1038/nrm2124

McKeegan, K.S., C.M. Debieux, S. Boulon, E. Bertrand, and N.J. Watkins. 2007. A dynamic scaffold of pre-snoRNP factors facilitates human box C/D snoRNP assembly. *Mol. Cell. Biol.* 27:6782–6793. http://dx.doi.org/10.1128/MCB.01097-07

McKeegan, K.S., C.M. Debieux, and N.J. Watkins. 2009. Evidence that the AAA+ proteins TIP48 and TIP49 bridge interactions between 15.5K and the related NOP56 and NOP58 proteins during box C/D snoRNP biogenesis. *Mol. Cell. Biol.* 29:4971–4981. http://dx.doi.org/10.1128/MCB.00752-09

Meister, G., D. Bühler, R. Pillai, F. Lottspeich, and U. Fischer. 2001. A multiprotein complex mediates the ATP-dependent assembly of spliceosomal U snRNPs. *Nat. Cell Biol.* 3:945–949. http://dx.doi.org/10.1038/ncb1101-945

Newman, D.R., J.F. Kuhn, G.M. Shanab, and E.S. Maxwell. 2000. Box C/D snoRNA-associated proteins: two pairs of evolutionarily ancient proteins and possible links to replication and transcription. *RNA*. 6:861–879. http://dx.doi.org/10.1017/S1355838200992446

Oruganti, S., Y. Zhang, and H. Li. 2005. Structural comparison of yeast snoRNP and spliceosomal protein Snu13p with its homologs. *Biochem. Biophys. Res. Commun.* 333:550–554. http://dx.doi.org/10.1016/j.bbrc.2005.05.141

Pal, M., M. Morgan, S.E. Phelps, S.M. Roe, S. Parry-Morris, J.A. Downs, S. Polier, L.H. Pearl, and C. Prodromou. 2014. Structural basis for phosphorylation-dependent recruitment of Tel2 to Hsp90 by Pih1. *Structure*. 22:805–818. http://dx.doi.org/10.1016/j.str.2014.04.001

Peng, W.T., M.D. Robinson, S. Mnaimneh, N.J. Krogan, G. Cagney, Q. Morris, A.P. Davierwala, J. Grigull, X. Yang, W. Zhang, et al. 2003. A panoramic view of yeast noncoding RNA processing. *Cell*. 113:919–933. http://dx.doi.org/10.1016/S0092-8674(03)00466-5

Rothé, B., R. Back, M. Quinternet, J. Bizarro, M.C. Robert, M. Blaud, C. Romier, X. Manival, B. Charpentier, E. Bertrand, and C. Branlant. 2014. Characterization of the interaction between protein Snu13p/15.5K and the Rsa1p/NUFIP factor and demonstration of its functional importance for snoRNP assembly. *Nucleic Acids Res.* 42:2015–2036. http://dx.doi.org/10.1093/nar/gkt1091

Schultz, A., S. Nottrott, N.J. Watkins, and R. Lührmann. 2006. Protein-protein and protein-RNA contacts both contribute to the 15.5K-mediated assembly of the U4/U6 snRNP and the box C/D snoRNPs. *Mol. Cell. Biol.* 26:5146–5154. http://dx.doi.org/10.1128/MCB.02374-05

Terns, M., and R. Terns. 2006. Noncoding RNAs of the H/ACA family. *Cold Spring Harb. Symp. Quant. Biol.* 71:395–405. http://dx.doi.org/10.1101/sqb.2006.71.034

Terwilliger, T.C. 2000. Maximum-likelihood density modification. *Acta Crystallogr. D Biol. Crystallogr.* 56:965–972. http://dx.doi.org/10.1107/S0907444900005072

Terwilliger, T.C., and J. Berendzen. 1999. Automated MAD and MIR structure solution. *Acta Crystallogr. D Biol. Crystallogr.* 55:849–861. http://dx.doi.org/10.1107/S0907444999000839

Tosi, A., C. Haas, F. Herzog, A. Gilmozzi, O. Berninghausen, C. Ungewickell, C.B. Gerhold, K. Lakomek, R. Aebersold, R. Beckmann, and K.P. Hopfner. 2013. Structure and subunit topology of the INO80 chromatin remodeler and its nucleosome complex. *Cell*. 154:1207–1219. http://dx.doi.org/10.1016/j.cell.2013.08.016

Vagin, A.A., R.A. Steiner, A.A. Lebedev, L. Potterton, S. McNicholas, F. Long, and G.N. Murshudov. 2004. REFMAC5 dictionary: organization of prior chemical knowledge and guidelines for its use. *Acta Crystallogr. D Biol. Crystallogr.* 60:2184–2195. http://dx.doi.org/10.1107/S0907444904023510

Verheggen, C., D.L. Lafontaine, D. Samarsky, J. Mouaikel, J.M. Blanchard, R. Bordonné, and E. Bertrand. 2002. Mammalian and yeast U3 snoRNPs are matured in specific and related nuclear compartments. *EMBO J.* 21:2736–2745. http://dx.doi.org/10.1093/emboj/21.11.2736

Vidovic, I., S. Nottrott, K. Hartmuth, R. Lührmann, and R. Ficner. 2000. Crystal structure of the spliceosomal 15.5kD protein bound to a U4 snRNA fragment. *Mol. Cell*. 6:1331–1342. http://dx.doi.org/10.1016/S1097-2765(00)00131-3

Walbott, H., R. Machado-Pinilla, D. Liger, M. Blaud, S. Réty, P.N. Grozdanov, K. Godin, H. van Tilbeurgh, G. Varani, U.T. Meier, and N. Leulliot. 2011. The H/ACA RNP assembly factor SHQ1 functions as an RNA mimic. *Genes Dev.* 25:2398–2408. http://dx.doi.org/10.1101/gad.176834.111

Wang, C., and U.T. Meier. 2004. Architecture and assembly of mammalian H/ACA small nucleolar and telomerase ribonucleoproteins. *EMBO J.* 23:1857–1867. http://dx.doi.org/10.1038/sj.emboj.7600181

Watkins, N.J., and M.T. Bohnsack. 2012. The box C/D and H/ACA snoRNPs: key players in the modification, processing and the dynamic folding of ribosomal RNA. *Wiley Interdiscip Rev RNA*. 3:397–414. http://dx.doi.org/10.1002/wrna.117

Watkins, N.J., V. Ségault, B. Charpentier, S. Nottrott, P. Fabrizio, A. Bachi, M. Wilm, M. Rosbash, C. Branlant, and R. Lührmann. 2000. A common core RNP structure shared between the small nucleoar box C/D RNPs and the spliceosomal U4 snRNP. *Cell*. 103:457–466. http://dx.doi.org/10.1016/S0092-8674(00)00137-9

Watkins, N.J., A. Dickmanns, and R. Lührmann. 2002. Conserved stem II of the box C/D motif is essential for nucleolar localization and is required, along with the 15.5K protein, for the hierarchical assembly of the box C/D snoRNP. *Mol. Cell. Biol.* 22:8342–8352. http://dx.doi.org/10.1128/MCB.22.23.8342-8352.2002

Watkins, N.J., I. Lemm, D. Ingelfinger, C. Schneider, M. Hossbach, H. Urlaub, and R. Lührmann. 2004. Assembly and maturation of the U3 snoRNP in the nucleoplasm in a large dynamic multiprotein complex. *Mol. Cell*. 16:789–798. http://dx.doi.org/10.1016/j.molcel.2004.11.012

Winn, M.D., C.C. Ballard, K.D. Cowtan, E.J. Dodson, P. Emsley, P.R. Evans, R.M. Keegan, E.B. Krissinel, A.G. Leslie, A. McCoy, et al. 2011. Overview of the CCP4 suite and current developments. *Acta Crystallogr. D Biol. Crystallogr.* 67:235–242. http://dx.doi.org/10.1107/S0907444910045749

Xue, S., R. Wang, F. Yang, R.M. Terns, M.P. Terns, X. Zhang, E.S. Maxwell, and H. Li. 2010. Structural basis for substrate placement by an archaeal box C/D ribonucleoprotein particle. *Mol. Cell*. 39:939–949. http://dx.doi.org/10.1016/j.molcel.2010.08.022

Ye, K., R. Jia, J. Lin, M. Ju, J. Peng, A. Xu, and L. Zhang. 2009. Structural organization of box C/D RNA-guided RNA methyltransferase. *Proc. Natl. Acad. Sci. USA*. 106:13808–13813. http://dx.doi.org/10.1073/pnas.0905128106

Yong, J., M. Kasim, J.L. Bachorik, L. Wan, and G. Dreyfuss. 2010. Gemin5 delivers snRNA precursors to the SMN complex for snRNP biogenesis. *Mol. Cell*. 38:551–562. http://dx.doi.org/10.1016/j.molcel.2010.03.014

Zhang, R., B.R. So, P. Li, J. Yong, T. Glisovic, L. Wan, and G. Dreyfuss. 2011. Structure of a key intermediate of the SMN complex reveals Gemin2's crucial function in snRNP assembly. *Cell*. 146:384–395. http://dx.doi.org/10.1016/j.cell.2011.06.043

Zhao, R., M. Davey, Y.C. Hsu, P. Kaplanek, A. Tong, A.B. Parsons, N. Krogan, G. Cagney, D. Mai, J. Greenblatt, et al. 2005. Navigating the chaperone network: an integrative map of physical and genetic interactions mediated by the hsp90 chaperone. *Cell*. 120:715–727. http://dx.doi.org/10.1016/j.cell.2004.12.024

Zhao, R., Y. Kakihara, A. Gribun, J. Huen, G. Yang, M. Khanna, M. Costanzo, R.L. Brost, C. Boone, T.R. Hughes, et al. 2008. Molecular chaperone Hsp90 stabilizes Pih1/Nop17 to maintain R2TP complex activity that regulates snoRNA accumulation. *J. Cell Biol.* 180:563–578. http://dx.doi.org/10.1083/jcb.200709061